Global and Planetary Change 127 (2015) 34–49

Contents lists available at ScienceDirect

Global and Planetary Change

journal homepage: www.elsevier.com/locate/gloplacha

Alpine topography in the light of tectonic uplift and glaciation

Jörg Robl [a,*], Günther Prasicek [b], Stefan Hergarten [c], Kurt Stüwe [d]

[a] University of Salzburg, Geography and Geology, Salzburg, Austria
[b] University of Salzburg, Geoinformatics — Z_GIS, Salzburg, Austria
[c] University of Freiburg, Earth and Environmental Sciences, Freiburg, Germany
[d] University of Graz, Earth Sciences, Graz, Austria

ARTICLE INFO

Article history:
Received 30 June 2014
Received in revised form 14 November 2014
Accepted 14 January 2015
Available online 22 January 2015

Keywords:
European Alps
Slope–elevation distribution
Slope stability
Glacial buzz-saw
Premature landscape

ABSTRACT

In steady-state orogens, topographic gradients are expected to increase with elevation whereas the European Alps feature a transition from increasing to decreasing slopes. This peculiar pattern has been interpreted to reflect either the critical slope stability angle or a premature fluvial landscape but is also consistent with the glacial buzz-saw hypothesis. To disentangle the contributions of each of these principles we split the Alps into contiguous domains of structural units and analyze their slope–elevation distributions emphasizing glaciated and non-glaciated realms. In comparable structural units within the extent of the last glacial maximum (LGM) the transition from increasing to decreasing slopes is located at the equilibrium line altitude (ELA) of the LGM and we interpret this to be evidence for the impact of glacial erosion. Decay rates of glacial landforms towards steady-state slopes depend on lithological properties leading to a landscape characterized by different transient states. Beyond the LGM limits the slope–elevation distributions show local maxima as well, but these are located at varying altitudes implying a tectonic driver. This observation and data from surrounding basins suggests that at least parts of the European Alps experienced a pre-Pleistocene pulse of tectonic uplift. The resulting presence of premature low-gradient terrain above the ELA during the global cooling in Plio–Pleistocene times would have heavily influenced the onset and the extent of an alpine ice cap.

1. Introduction

The topography of the European Alps reflects continental collision, crustal thickening, and buoyancy driven surface uplift overprinted by erosional processes following topographic gradients (e.g. Ratschbacher et al., 1991; Frisch et al., 1998; Robl et al., 2008b; Luth et al., 2013). These processes act on individual spatial and temporal scales and should in principle be identifiable in the resulting landforms. However, superposition, spatially non-uniform rates and different timing of these processes, feedback loops between lithospheric and surface processes, and the state of (non)-equilibrium of landforms still drive the debate on the formation of topography and relief in terms of uplift and erosion in the European Alps (Hergarten et al., 2010; Norton et al., 2010; Wagner et al., 2010; Sternai et al., 2012).

1.1. Formation and destruction of topography in the Alps

The indentation of the Adriatic micro plate with Europe caused spatially and temporally variable uplift as a consequence of a complex deformation field due to contrasting rheological properties of crustal blocks, large scale fault systems, and the Mid-Miocene stress field inversion (e.g. Robl et al., 2008b). Deep-seated mantle processes such as slab breakoff or the delamination of the mantle part of the lithosphere might also be responsible for recent large scale uplift due to increased buoyancy of the European Alps (Lyon-Caen and Molnar, 1989; von Blankenburg and Davis, 1995; Duretz et al., 2011; Valera et al., 2011). This leads to the formation of relief over time which is expressed by increasing topographic gradients and potential energy.

Simultaneously to uplift, gravity-driven erosional surface processes act along the topographic gradients and remove newly formed topography until a morphological steady-state is established where uplift and erosion rates are balanced (Montgomery, 2001). The drainage system represents the backbone of the alpine landscape and is responsible for bed rock erosion and the long range transport of rocks as bed load, suspension or solution downstream towards the foreland basins (e.g. Hinderer et al., 2013). Hillslopes constitute the largest parts of a mountain landscape where the drainage system sets the lower boundary condition for the hillslope evolution over time. Hillslope gradients adjust to river incision by mass wasting towards steady-state hillslope angles (Strahler, 1950; Montgomery, 2001). Gradients in channels and hillslopes are controlled by the erosional resistance of the lithology suggesting that rock properties are a first-order control on the topographic evolution of a mountain range.

* Corresponding author at: Dept. Geography and Geology University of Salzburg Hellbrunnerstraße 34/III 5020 Salzburg Tel.: +43 (0) 662 8044 5419.
E-mail address: joerg.robl@sbg.ac.at (J. Robl).

http://dx.doi.org/10.1016/j.gloplacha.2015.01.008
0921-8181/

Mass wasting along hillslopes, bed rock incision in drainage systems and glacial scouring are conditioned by the climate (e.g. Norton et al., 2010). A globally recorded cooling trend initiated in Pliocene times (e.g. Zachos et al., 2001) and culminated in the Pleistocene glaciation cycles. During these glacial stages, a predominant part of the European Alps was covered by an ice cap and the landscape was reshaped by glacial erosion (e.g. Penck, 1905). Consequently, glacial landforms like cirques and glacial troughs are abundant throughout the Alps (e.g. van der Beek and Bourbon, 2008) representing transient landscapes during inter- and postglacial periods (Norton et al., 2008; Salcher et al., 2014). As a consequence, the geometry of the drainage system is characterized by a massive glacially-induced disturbance of former (steady-state?) longitudinal channel profiles in mountainous regions in the form of prominent knick points and the so-called "inner gorges" that have been preserved through repeated alpine glaciations (Montgomery and Korup, 2011). In addition, a horizontal shift of the main streams may occur due to both glacial erosion and increased sediment delivery (Robl et al., 2008a; Garzanti et al., 2011; Monegato and Vezzoli, 2011).

Extensive glacial dissection of the alpine landscape happened since around 0.87 Ma (Muttoni et al., 2003; Haeuselmann et al., 2007; Scardia et al., 2012) and resulted in base level lowering of several tens (and possibly hundreds) of meters in the main channels of the Western (Schlunegger and Schneider, 2005; Herman et al., 2011) and Eastern Alps (Preusser et al., 2010; Reitner et al., 2010). In addition, alpine base level changes are also related to spatial and temporal variable uplift rates (Wagner et al., 2010; Meyer et al., 2011; Legrain et al., 2014b) and the desiccation of the Mediterranean during the Messinian salinity crisis (e.g. Willett et al., 2006). Channels transfer the information on base level changes upstream by the migration of knick points that incise into the bed rock (e.g. Whipple et al., 2013), enter tributaries and trigger mass wasting processes at corresponding hillslopes (Schlunegger, 2002; Robl et al., 2008a; Schlunegger et al., 2009). This may cause an orogen-wide reorganization of the drainage system by the migration of divides and river piracy events (Stüwe et al., 2008; Willett et al., 2014). Again, the pace of landscape reorganization towards steady-state strongly depends on lithology (e.g. Hurst et al., 2013).

A feedback between tectonics and climate exists via erosional unloading of the orogen. Hillslopes locally transfer regolith to confining streams or glaciers which in turn transport mass from the mountains to the foreland basins unloading the orogen (e.g. Hinderer et al., 2013). The orogen responds with flexural isostatic uplift driven by erosion leading to the formation of additional relief (Gudmundsson, 1994; Wittmann et al., 2007; Champagnac et al., 2009; Scardia et al., 2012). In contrast to tectonically controlled uplift, peaks are rising but the mean elevation and potential energy of the orogen decrease in sum of erosion and isostatic surface uplift (Wager, 1937; Szekely, 2003; Champagnac et al., 2007).

Kuhlemann et al. (2002) discovered a massive increase of sediment delivery from the European Alps caused by erosion rates approximately doubling since around 5 Ma and posed the question on climatic or tectonic drivers. This observation is consistent with the low temperature thermochronology from the Western and Central Alps indicating a significant increase of exhumation rates within this time slice (Vernon et al., 2008). Whatever drivers (climate or tectonics) may have caused the increased denudation rates and sediment delivery, the alpine landscape is currently in a transient state and patterns of processes that adjust the alpine landscape towards a geomorphic equilibrium are recorded constantly as expression of alpine topography and can therefore be extracted by analyzing digital elevation models.

1.2. The topographic pattern in digital elevation models

Triggered by the pioneering morphometric studies of Frisch et al. (2000) and Szekely (2001) many authors analyzed digital elevation models (DEMs) of the Alps to infer tectonic, climatic and lithological conditioning from topographic gradients and channel slopes (e.g. Robl et al., 2008a).

Kühni and Pfiffner (2001) analyzed the topographic pattern in the Swiss Alps and discovered an increase of topographic gradients with increasing surface elevation up to 1500 m, followed by a constant average slope of about 25° up to 2900 m and a further steepening in the summit regions. They interpreted this pattern as the average limiting slope stability angle for the Swiss Alps that is in good agreement with the average slope of 25° reported by Schmidt and Montgomery (1995). The increase in slope at about 2900 m is interpreted as a combination of permafrost stabilizing the regolith cover of the slopes and the transition from a fluvial to a glacial erosional regime.

Hergarten et al. (2010) analyzed channel slopes at given catchment sizes instead of topographic gradients to avoid complications introduced by the non-linearity of the stream power formulation. They interpreted the increase of channel slopes with increasing surface elevation up to about 1500–2000 m and the decrease of channel slopes above as evidence for the morphological prematurity of the Alps caused by accelerated uplift since around 5 Ma. In fact, a recent large scale uplift event is documented at the periphery of the Alps and in adjacent basins (Wagner et al., 2010; Cederbom et al., 2011; Gusterhuber et al., 2012; Legrain et al., 2014a). This is consistent with the observed transient landscape of the inner Alps where the channel morphology of the lower regions may be interpreted as morphological equilibrium state of the recent pulse of uplift. Domains at high altitudes characterized by reduced channel gradients may represent lower uplift rates that have driven topography formation before this latest pulse of uplift.

Both studies present strong arguments in favor of their hypotheses with a consistent but not unique interpretation of the observed pattern. Alternatively, glacial erosion is thought to cause a similar slope distribution: Several studies describe a maximum in the hypsometric curve at the equilibrium line altitude (ELA) in regions characterized by a strong glacial impact (Brozović et al., 1997; Spotila et al., 2004; Egholm et al., 2009) and the formation of over-deepened valleys and glacial lakes with nearly vertical valley flanks (e.g. van der Beek and Bourbon, 2008). Hence, the shape of the hypsometric curve of the Alps may be caused by a decrease of mean elevation as a consequence of the "glacial buzz-saw" resulting in lower topographic gradients at and above the ELA and in the formation of valley scale relief due to glacial dissection below the ELA (e.g. Sternai et al., 2012).

The slope–elevation distribution of the Alps as observed by Kühni and Pfiffner (2001) and Hergarten et al. (2010) seems also consistent with and could therefore be caused by glacial erosion. The scope of this study is to disentangle the potential influence of prematurity, slope stability and glacial erosion on the peculiar topography of the European Alps.

1.3. Hypothetical slope–elevation effects of prematurity, slope stability and glacial sculpting

Each of the three geomorphological principles described above — morphological prematurity, slope stability and glacial erosion predicts an individual characteristic slope–elevation distribution (Fig. 1). Assuming a simplified mountain range with surface uplift rate linearly increasing towards the main divide (tent-shaped uplift rate), fluvial equilibrium is represented by an increase of average slope with surface elevation (Hergarten et al., 2010).

In case of prematurity, the slope–elevation distribution is characterized by a turning point from increasing to decreasing slope with elevation (Fig. 1a). However, spatial variations in uplift are unlikely for the small scale structural units investigated in this study. Here, we rather expect uniform uplift rates hence constant slopes over the entire elevation range in geomorphological equilibrium as long as the distribution of upstream drainage areas does not change significantly with altitude. Given uniform uplift, prematurity also features a turning point in the slope–elevation distribution separating high topographic gradients at low altitudes from low topographic gradients at high altitudes.

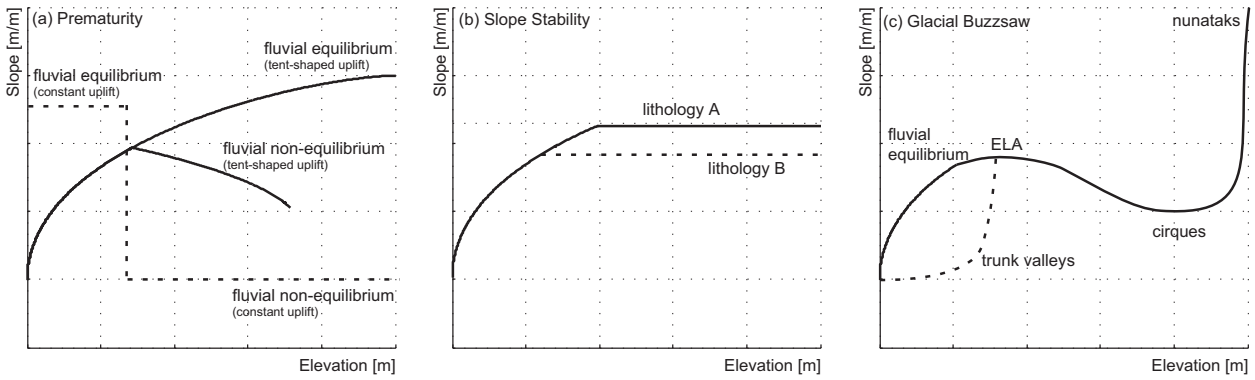

Fig. 1. Characteristic slope–elevation curves of the three proposed geomorphic concepts for the topography development of the European Alps: a) state of maturity (corresponding to Fig. 7 in Hergarten et al. (2010)), b) slope stability in a mature alpine landscape, and c) glacial buzz-saw.

A constant slope with increasing surface elevation can also be expected in rapidly uplifting fluvial areas where hillslopes reach the critical slope stability angle. The critical slope stability angle imposes a limit to the topographic gradients varying with the lithological inventory (Fig. 1b).

Glacial erosion alters fluvial topography in a characteristic way: at and above the ELA local relief is destroyed by the formation of glacial cirques (glacial buzz-saw) indicated by a decrease in topographic gradient, leaving nearly vertical cirque faces and nunataks in the summit regions; glaciated trunk valleys lead to a bimodal slope distribution below the ELA generally not recognized in standard slope–elevation plots where only the mean slope is considered as a function of elevation (Fig. 1c). An exceptional feature of this conceptual pattern is a transition from increasing to decreasing slope with surface elevation approximately located at the LGM ELA.

In the European Alps, the observed topography can be expected to be the result of these principles combined and the persistence of the topographic disequilibrium is controlled by surface process rates towards a new steady-state and therefore lithology-dependent. There is a consensus that this dependency represents a first-order control on the steepness of fluvial channels and hillslope gradients in steady-state and that the response time of a transient landscape is governed by lithology (Korup and Weidinger, 2011; Montgomery and Korup, 2011; Hurst et al., 2013).

In this study we employ a novel approach considering not only the mean slope at a given elevation, but also its statistical distribution. The method is applied to a set of contiguous domains of the major structural units of the European Alps (Bousquet et al., 2012) being characteristic for the three presented theoretical slope–elevation curves in order to interpret the topography of the orogen.

2. Data and methods

We follow the approach of Kühni and Pfiffner (2001) and Hergarten et al. (2010) and analyze the distribution of slope versus surface elevation of the European Alps (Fig. 2). Our analysis is based on version 4 of the freely available shuttle radar topography mission (SRTM) DEM with a resolution of 3 arc sec (Farr and Kobrick, 2000). SRTM tiles were mosaicked and projected to a Lambert Conformal Conic projection (EPSG: 3034) with a spatial resolution of 50 m. Slopes in m/m were calculated by the standard algorithm implemented in GRASS GIS (e.g. Neteler et al., 2012).

In contrast to previous studies we particularly focus on lithological and glacial influences. We first split the European Alps into homogenous domains characterized by their tectonic position and lithological inventory based on the map "Tectonic Framework of the Alps" (Bousquet et al., 2012). Subsequently, we analyze the slope–elevation relation for each segment and compare the results with special emphasis on lithology and glaciation.

Hergarten et al. (2010) suggest using channel slopes within a limited range of catchment sizes in order to avoid complications due to the nonlinear contributions of slope and drainage area to fluvial erosion in the stream power approach. The application of channel slopes for specific catchment sizes effectively removes the local topographic maxima at the very headwaters including the steepest parts of the Alps (peaks and ridges). However, the constraints of their analysis can be relaxed as results for channel slopes for specific catchment sizes and topographic gradients employed for this work provide similar information. This can be expected as cells holding a small upstream drainage area reflect both hillslope and fluvial process patterns and large catchments sizes have a minor influence on the slope–elevation distribution due to their low frequency of occurrence (McNamara et al., 2006). A major advantage of our approach is the visibility of both the findings of Kühni and Pfiffner (2001) and of Hergarten et al. (2010) at high altitudes. In extension of the studies of Kühni and Pfiffner (2001) and of Hergarten et al. (2010) our approach not only focuses on the mean slope at a given elevation and its variance, but also takes the shape of the slope distribution into account. In a first step, the data set consisting of slope–elevation pairs is subdivided into 50 m wide elevation slices, and the statistical distribution of the topographic slopes in each slice is evaluated individually. For a graphical representation of the distribution, the relative frequency of occurrence of slope values within each elevation slice is evaluated using 0.025 m/m wide bins. Mean values, standard deviations, and percentiles ($P_{15.9}$, P_{50} and $P_{84.1}$) are computed from the original slope values without binning. For a normal distribution of slopes within an elevation slice, the median value equals the mean value and the $P_{15.9}$ and $P_{84.1}$ percentiles correspond to the mean value ± 1 standard deviation, so that the provided statistics indicate the deviation from a Gaussian distribution.

3. Expressions of alpine topography

The slope–elevation distribution for the entire Alps shows the previously discussed pattern with an increase in slope up to about 1800 m followed by constant mean and median slopes of about 0.52 (~27°) up to about 2900 m (Fig. 2). From there, the mean and median topographic gradients increase up to 0.8 (~39°) at summit regions (Fig. 2c, white and magenta circles). The strongest increase in slope occurs from the valley floors up to about 1000 m. These findings were described by Kühni and Pfiffner (2001). However, the behavior of mean and median slopes in high altitudes coincides with the occurrence of slopes beyond 0.8 (39°) and with mode values (Fig. 2c, white triangles) decreasing with increasing surface elevation — the pattern described by Hergarten et al. (2010). While the mode values show considerable scatter this trend is clearly depicted by the frequency density. These observations

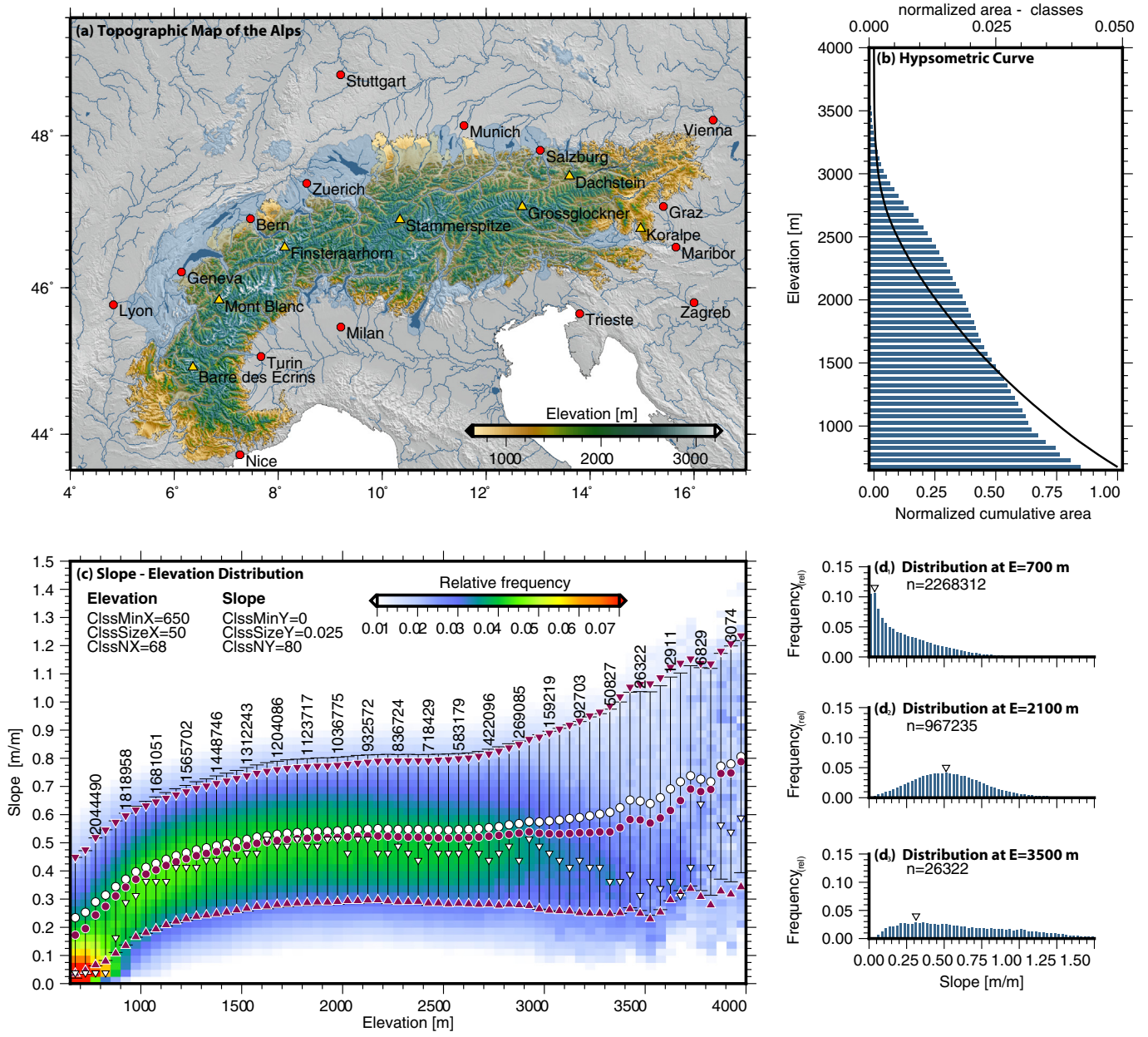

Fig. 2. Topographic pattern of the European Alps: (a) Topographic map of the orogen color coded for surface elevation above 650 m. The 650 m elevation cutoff conforms to the threshold employed by Hergarten et al. (2010) to allow for direct comparison. Red circles and yellow triangles indicate the position of important cities and peaks, respectively. The extent of the LGM is shown by light blue transparent polygons. The drainage system and important lakes are displayed as blue lines and dark blue polygons. (b) The hypsometric curve of the European Alps above 650 m is represented by the black solid line. Blue bars indicate the normalized area of each elevation class. (c) Slope–elevation distribution for the entire European Alps above 650 m. White circles and black error bars indicate the mean slope and one standard deviation for each 50 m elevation slice. Magenta circles show the median values and magenta triangles indicate the 15.8 and 84.1 percentiles so that the range between the triangles includes 68.3% of the data. White triangles mark the mode values for each elevation slice. The number of cells of every third elevation slice is annotated. Histograms (d_1)–(d_3) show the frequency of slopes at E = 700 m, E = 2100 m, and E = 3500 m, respectively, and white triangles indicate the mode values. Note that histograms represent vertical sections in the slope–elevation space at the indicated elevation slice. (For interpretation of the references to color in this figure legend, the reader is referred to the web version of this article.)

are also represented in the histograms that show the distribution of slopes at specific elevation slices (Fig. 2d_1–d_3). At low elevations (E = 700 m) we have a maximum at very low slopes and an exponential decline towards high topographic gradients (Fig. 2b). At E = 2100 m the distribution is characterized by a maximum at slope values around 0.5 and a decrease in frequency towards larger and smaller slopes. The distribution is slightly skewed right. At E = 3500 m the distribution is considerable skewed towards very large slopes (Fig. 2d_1–d_3).

The slope–elevation distribution of the entire Alps derived by the methodology outlined above is consistent with the observations and interpretations of Kühni and Pfiffner (2001) (mean and median values), as well as Hergarten et al. (2010) (density and mode values), but may also be explained by glacial erosion (Fig. 1). The bulge in the hypsometric curve roughly at the LGM ELA is equivalent to reduced topographic gradients and is interpreted as the characteristic pattern of a landscape coined by the "glacial buzz-saw" (Egholm et al., 2009). However, as outlined in Fig. 1a, slopes decreasing with surface elevation can also be an expression of a premature landscape. An exclusive statement on the prevailing process can therefore not be derived from a single Alps-wide analysis as it is biased by the very heterogeneous lithological inventory and the glacial history of the mountain range. In addition, a possible recent pulse of uplift may be characterized by spatiotemporal variability. Hence, we explore the isolated effects of prematurity, slope stability, and glaciation on the topography by analyzing the slope–

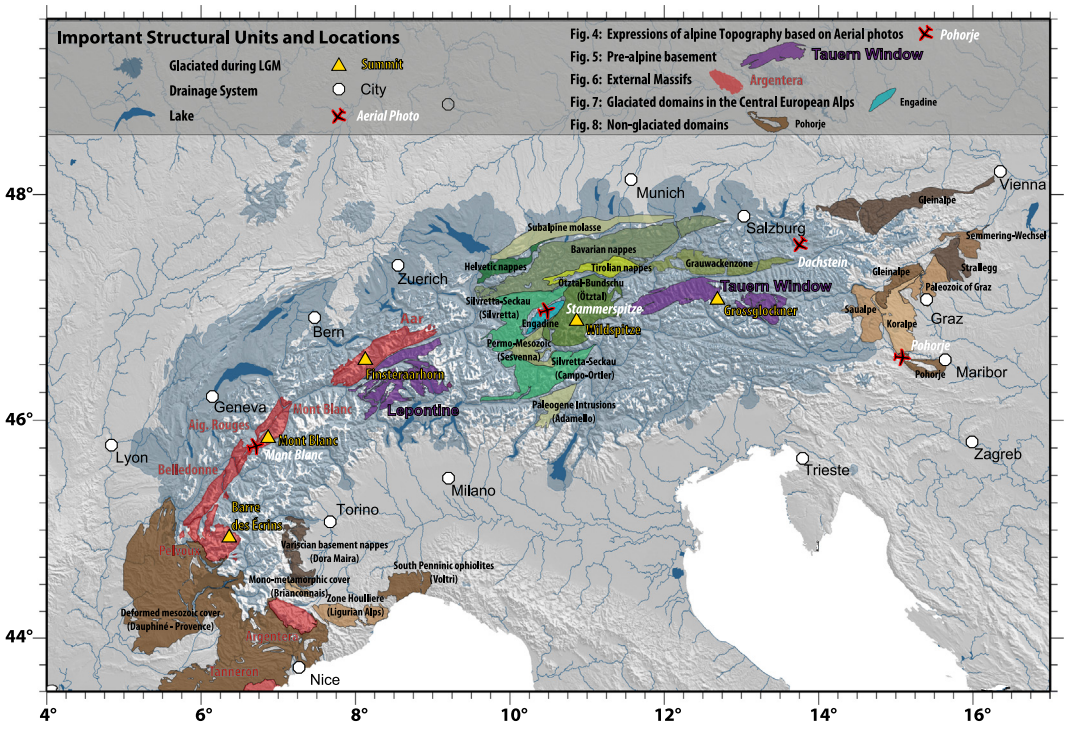

Fig. 3. Important structural units and locations: Spatial position of all analyzed contiguous domains of the main structural units of the Alps described in this study and links to figures depicting the slope–elevation distributions of these domains in detail. The position of aerial photos, important cities, summits, lakes, and drainages systems are plotted for orientation.

elevation distribution of homogenous domains of the major structural units of the European Alps individually (Fig. 3).

Field observations clearly illustrate that areas characterized by different lithology host different landforms and that the glaciated domains of the Alps differ significantly in their appearance from domains without glacial impact (Fig. 4). Therefore, we begin our analysis by confronting qualitative landscape observations of four iconic regions from the Western and Eastern Alps with their slope–elevation distributions. These four regions were selected to represent alpine landscapes characterized by (3.1) glacial imprint and high landform persistence, (3.2) glacial imprint and low landform persistence, (3.3) low surface process rates due to karstification and subsurface run-off and (3.4) fluvial landscape prematurity caused by a recent pulse of uplift.

3.1. Glaciated with high landform persistence: the Mont Blanc Massif

The Mont Blanc Massif consists predominantly of polyphase, high grade metamorphic rocks and is representative for an alpine landscape with strong glacial imprint. While lower elevation slices are characterized by trunk valleys including active glacial erosion above 1800 m, spacious areas at higher altitudes are occupied by cirques bordered by very steep ridges and horns (Figs. 3, 4a). This qualitative description is well in line with the observed slope–elevation distribution for the Mont Blanc Massif region as outlined in Fig. 3 and shown in Fig. 4a (inset) and also consistent with the proposed hypothetical slope–elevation curve for a glaciated landscape (Fig. 1c). Trunk valleys at lower altitudes imply a bimodal landscape characterized by a high frequency of occurrence for both high and low slopes in the slope–elevation distribution. The mode of the slope distribution is the largest in the elevation slices between 1500 and 2000 m and roughly coincides with the position of the LGM ELA (Ivy-Ochs et al., 2006, 2008). From this elevation range onwards — the lower limit where spacious cirques are observed — the topographic gradients decrease with increasing surface elevation. Over the entire distribution, the standard deviation of the slopes exceeds 0.2 due to the occurrence of very steep landscape patches with slope values above 1 representing trunk valley flanks, cirque faces, and ridges. At summit regions these ridges, faces, and horns become predominant relative to the cirque floors causing an increase of the mean and median slope values. Nevertheless, the modal slope values further decrease with increasing surface elevation up to about E = 3800 m, but towards the highest peaks a rapid increase to mode values exceeding 0.8 can be observed which is well in line with the slope characteristics for the nunataks realm proposed in Fig. 1c. However, data scarcity in the highest elevation slices reduces the reliability of the related signals.

3.2. Glaciated with low landform persistence: the Engadin Window

The Engadin Window with peaks above 3000 m (e.g. Stammerspitze, Figs. 3, 4b) is located at the transition from the Western to the Eastern Alps in the center of the orogen — a region that was intensely glaciated several times during the Pleistocene. However, the landscape characteristics of this area differ significantly from those of the Mont Blanc Massif. The surface is dissected by numerous gullies and channels indicating water as the driving agent of erosion. Relics of glacial landforms have widely vanished and are observed only locally in areas of recent glaciation. In general, the landscape steepens with increasing surface elevation towards the highest summits of the Engadin Window like the Stammerspitze (Piz Tschütta).

This characteristic is quantitatively shown in the slope–elevation distribution that starts with very low topographic gradients at the valley floor of the Inn River (Fig. 4b, inset). The landscape steepens along the glacially sculpted flanks of the Inn valley and reaches a maximum in slope at about 1100 m followed by planation surfaces (valley shoulders) occurring at about 1300 m. From there on, the topographic gradients (mode values) increase continuously with elevation up to the summit regions with an accelerated increase in slope from 2600 m onwards. The mean slope also indicates a slope maximum at 1100 m but does not signify the planation surfaces of the valley shoulders due to a bimodal slope distribution in the respective elevation range. From 1300 m to 2700 m the mean slope increases only slightly but is followed by a strong increase towards the highest peaks of the area. While the Mont Blanc Massif features a wide range of topographic gradients

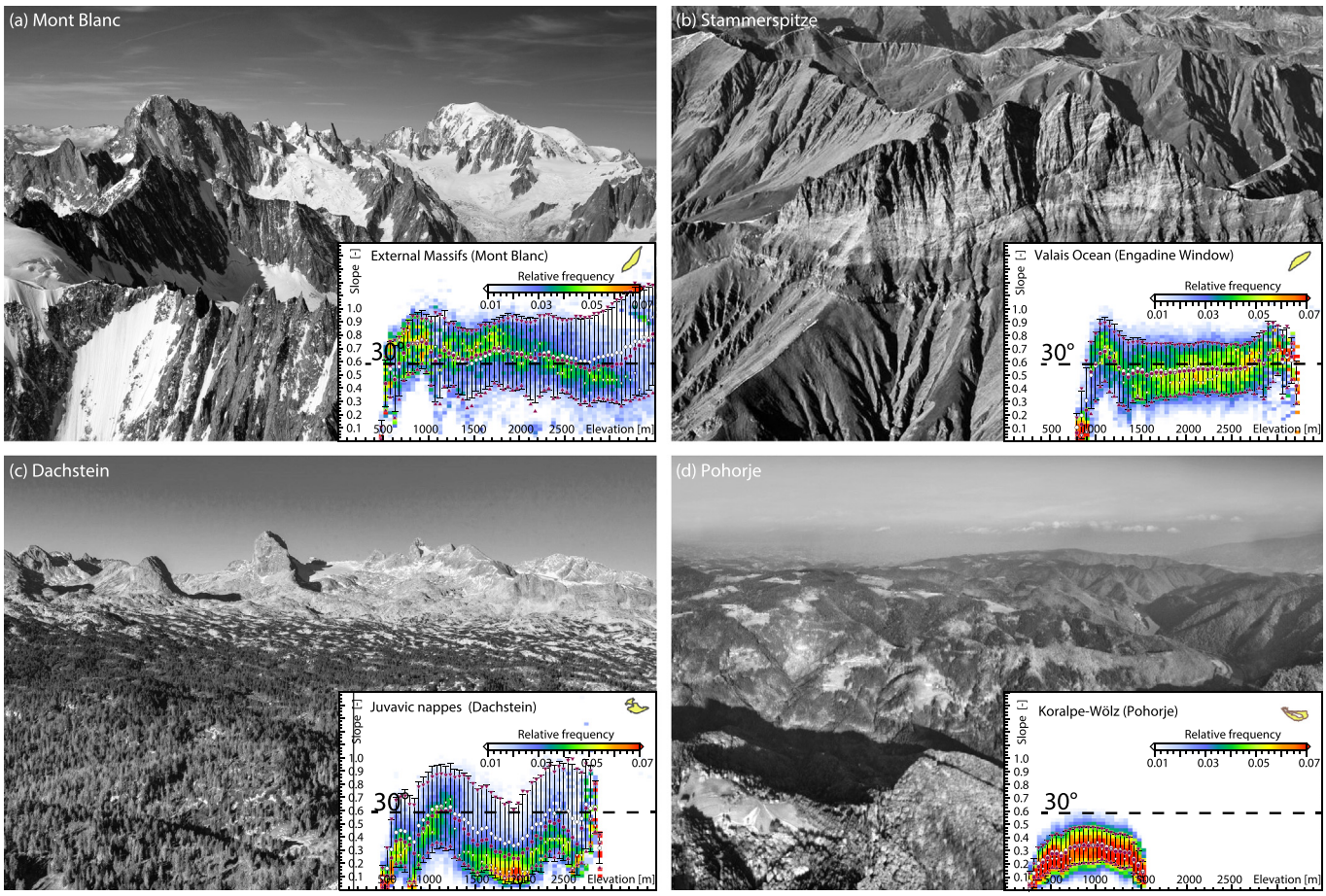

Fig. 4. Expressions of alpine topography shown in aerial photos from www.alpengeologie.org (Stüwe and Homberger, 2012) and corresponding slope–elevation distributions as insets. (a) Mont Blanc (b) Stammerspitze (c) Dachstein and (d) Koralpe. Note that a similar photo of the Dachstein—Augenstein landscape was presented by Frisch et al. (2000) and Frisch et al. (2001).

caused by ridges and peaks (high slopes) and cirque and trunk floors (low slopes), the slope–elevation distribution of the Engadin Window generally shows lower slopes and a reduced standard deviation. The lack of a glacial pattern in the Engadin Window nourishes the suspicion that the decay of glacial landforms happens at higher rates (and has probably started slightly earlier) as in the Mont Blanc Massif. In accordance to the concept of slope stability the persistence of non-equilibrium landforms in the Engadin Window is lower than in the Mont Blanc Massif and therefore highly lithology-dependent.

3.3. Regions with low surface process rates: the Dachstein Massif

The Dachstein Massif belongs to the glaciated part of the Northern Calcareous Alps (NCA) and shows outstanding morphological features that are not observed in the two examples described above, but are representative for this structural unit: planation surfaces and vertical faces (Figs. 3, 4c). The "upper planation surface", the so called Augenstein landscape at about 2000 m, is well known for hosting fluvial gravels of Oligocene to Miocene age (Frisch et al., 2001). A second Enns-valley parallel planation surface at about 1000 m is observed, but its age and significance in terms of landscape evolution are still unclear (Frisch et al., 2000; Keil and Neubauer, 2011). The two planation surfaces are separated by vertical faces especially at the southern boundary of the Massif. These field observations are consistent with the slope–elevation distribution of the area outlined as "Dachstein" in Fig. 3. While the low gradient elevation slices at about 500 m and 700 m mark the valley floors north and south of the Dachstein Massif, respectively, the landscape is strongly bimodal between 900 m and 1400 m. Within this elevation range spacious planation surfaces and steep near-vertical faces occur, featuring highest mean and modal slopes. The abundance of very low slopes between 1400 and 2100 m represents a paleo-surface, the dominant morphological feature in this elevation range. Beyond the plateau of the Augenstein landscape the relief steepens up to about 2500 m but the average slope decreases again towards the still glaciated regions near the summit. The persistence of paleo-surfaces and the lack of a fluvial erosion pattern can be attributed to the extensive karstification and missing surface run-off, which is a widespread phenomenon in the NCA and another example for lithology-dependent morphology.

3.4. Never glaciated regions at the fringe of the Alps: the Pohorje Massif

The Pohorje at the south-eastern border of the Eastern Alps was never glaciated during the Pleistocene glaciation cycles. It consists also of high grade metamorphic rocks of the Koralpe-Wölz nappe system and a plutonic body (granodioritic to tonalitic composition) of Miocene age that outcrops in the center of the range (Figs. 3, 4d). The Pohorje is split into a northern and southern domain by the deeply incised gorge of the Drava River. As the range does not consist of karstifiable rocks, surface run-off prevails and causes steep, incised channels at lower elevations separated by knick points from gentle headwaters at higher altitudes where a spacious paleo-surface occurs (Robl et al., 2008a) (Fig. 4d). The observation of a smooth and gentle landscape is consistent with the generally low slopes for this domain as implied by the slope–elevation distribution (Fig. 4d inset). The mean slopes for almost the entire elevation range are far below the critical slope stability angle. Here we discover a strong increase in slope from 300 to 500 m followed by

a significant drop in the mean and mode values of slope in the elevation range between 500 und 700 m. This low gradient surface coincides exactly in altitude with the occurrence of a dry and wide Drava River parallel valley (Ribnica basin). The average topographic gradients increase again to the highest values at about 1000 m. This is consistent with the observation of deeply incised channels (perpendicular to the dry valley) and steep corresponding hillslopes in this elevation range. This maximum in slope is followed by a significant decrease towards to the highest peaks where the landscape is composed of spacious and gentle paleo-surfaces covered abundantly by moorlands. Interestingly, the corresponding reduced slope angles at higher elevations are also characteristic for glaciated domains (e.g. Mont Blanc Massif). However, here they occur far below the alpine LGM ELA (Ivy-Ochs et al., 2008) and can therefore not be explained by glacial erosion. Moreover, a high standard deviation in slope related to glacial troughs and cirques as observed in the Mont Blanc area is missing in the Pohorje. Effects related to slope stability can be ruled out as well because observed topographic gradients are generally below the critical slope stability angle. Conversely, the morphology of the landscape is consistent with a premature state that was proposed for the entire European Alps (Hergarten et al., 2010) and may therefore be related to a recent pulse of uplift (Figs. 4d, 1a).

In summary, the four characteristic landscape types demonstrate a high landform diversity caused by glacial sculpting, tectonic uplift and variable persistence of transient landforms controlled by lithology.

4. Quantitative analysis of glacial, lithological and tectonic effects

The analysis of the four iconic landscapes that are frequently observed in the European Alps correlate well with the hypothetical slope–elevation curves discussed in Fig. 1. The presence of glacial morphology (e.g. cirques) coincides with pronounced deviations in the slope–elevation distribution from the hypothetical steady-state (Fig. 1a): a decrease of topographic gradients with increasing surface elevation is observed at higher altitudes. However, deviations are also observed in the non-glaciated parts of the Alps indicating prematurity. In the following sections we systematically explore the slope–elevation distribution of numerous contiguous domains of the main structural units of the European Alps and interpret their slope–elevation patterns in terms of (4.1) glacial effects, (4.2) lithological effects and (4.3) tectonic effects.

4.1. Glacial effects

As described in several studies (e.g. Frisch et al., 2000) and indicated by the four examples presented above, the lithological inventory, glacial imprint, and uplift history are controlling parameters of the topographic expression of the European Alps. Consequently, the morphological characteristics of regions at various positions within the orogen should be similar as long as lithological properties, glacial imprint, and latest tectonic history are comparable. To proof this assumption we explore the topographic expression of the Pre-alpine basement and the External Massifs that can be directly compared in terms of their structural position, lithological inventory and glacial history but are spatially distributed over several hundred kilometers from the Western to the Eastern Alps (Fig. 3).

4.1.1. The Pre-alpine basement at various spatial positions

Here we compare the slope–elevation distribution of the Tauern Window in the Eastern Alps with the Lepontine which is located in the Western Alps. Both areas belong to the “Pre-alpine basement” of the European Continent, but are about 250 km apart from each other (Figs. 3, 5). The Pre-alpine basement is part of the metamorphic nappes from the distal European margin. It consists of high grade metamorphic rocks and covers the center of the Tauern Window and large domains of the Lepontine (Fig. 5a). In addition, this domain represents a characteristic alpine landscape featuring persistent imprint of past glaciations. The slope-elevation distributions are consistent, both internally (e.g. western and eastern Tauern Window) and between the Lepontine and the Tauern Window area. In addition, they show the same pattern as the lithologically and glacially similar Mont Blanc Massif (Figs. 5b, c, 4a). The largest areas of the Pre-alpine basement units are located at a surface elevation between 2000 and 2500 m (Fig. 5d). The highest slopes occur at about 1500 m and decrease with increasing surface elevation up to 2600 m. At about 2900 m there is a second maximum in the slope–elevation distribution. From here to the summit region the slopes decrease again. This trend is clearly visible in the three histograms showing the frequency of slopes at the 400 m, the 1600 m, and the 2800 m elevation slices (Fig. 5d_1–d_3).

Gentle slopes are dominant at low elevations but their frequency of occurrence decreases rapidly with increasing surface elevation. The frequency distribution of slopes at 1600 m looks like a Gaussian distribution at the first glance but features two distinct deviations: the distribution is bimodal with one maximum at 0.55 and a second at 0.65 (Fig. 5d_2). In addition, the distribution is slightly right-skewed towards large slopes. The distribution becomes increasingly skewed towards large slopes with increasing surface elevation as shown at the 2800 m elevation slice. Here, the mode value of the highest frequency is shifted to 0.48 and the distribution shows a long tail towards slopes above 1.

The western Tauern Window and the western Lepontine (Antigorio) are large and continuous areas consisting of Pre-alpine basement rocks and are depicted in detail in Fig. 5e, f. Both domains show the same characteristics in the slope–elevation distribution with an increase of slopes with increasing surface elevation up to about 1500 m, followed by an upward decrease of mean slopes. Both domains include substantial areas with an average slope above 30°. These slopes are located between 1200 and 2200 m and between 800 and 2000 m in the Western Tauern Window and the Antigorio, respectively.

4.1.2. The External Massifs at various spatial positions

The External Massifs, as part of the Helvetic nappes, belong to the European Continent and can be directly compared to the Pre-alpine basement in terms of their tectonostratigraphic position, lithology, and glacial history. The polyphase crystalline rocks of the External Massifs break through the Mesozoic sedimentary cover at the peripheral part of the Western Alps (Figs. 3, 6). Interestingly, some of the highest peaks of the Alps including the Mont Blanc are located tens of kilometers north of the Alpine main divide. Here we explore the slope–elevation distribution of several External Massifs at various spatial positions that reflect landform diversity from the highly glaciated Aar- and Mont Blanc Massif to the slightly glaciated Argentera Massif in the northern and southern part of the Western Alps, respectively (Fig. 6a).

The highest mode values for slope occur at the 1800 m elevation slice marking a local maximum in the slope–elevation distribution followed by a decrease of slope with elevation (Fig. 6b). A damped but similar trend is observed in the mean and median slopes. However, at elevations above 3000 m the mode values further decrease upwards, while the occurrence of very steep landscape patches expressed by the high standard deviation causes an increase in mean slope with altitude. Along with the statistical measures the eye-catching similarities in the topographic expressions of the External Massifs and the Pre-alpine basement units support the assumption of a lithology- and glacial imprint-controlled topography of the European Alps. The Aar, Mont Blanc, Aiguille Rouges, Pelvoux-Ecrins, and Argentera Massifs undoubtedly show the transition from increasing to decreasing slopes with surface elevation roughly between 1500 and 2000 m. However, this trend is less clear with only mode values peaking slightly below 2000 m in the two analyzed domains of the Belledonne Massif. This could be explained by varying fractions of outcropping rock types composing the lithological inventory (e.g. Raumer et al., 1993). A significantly different

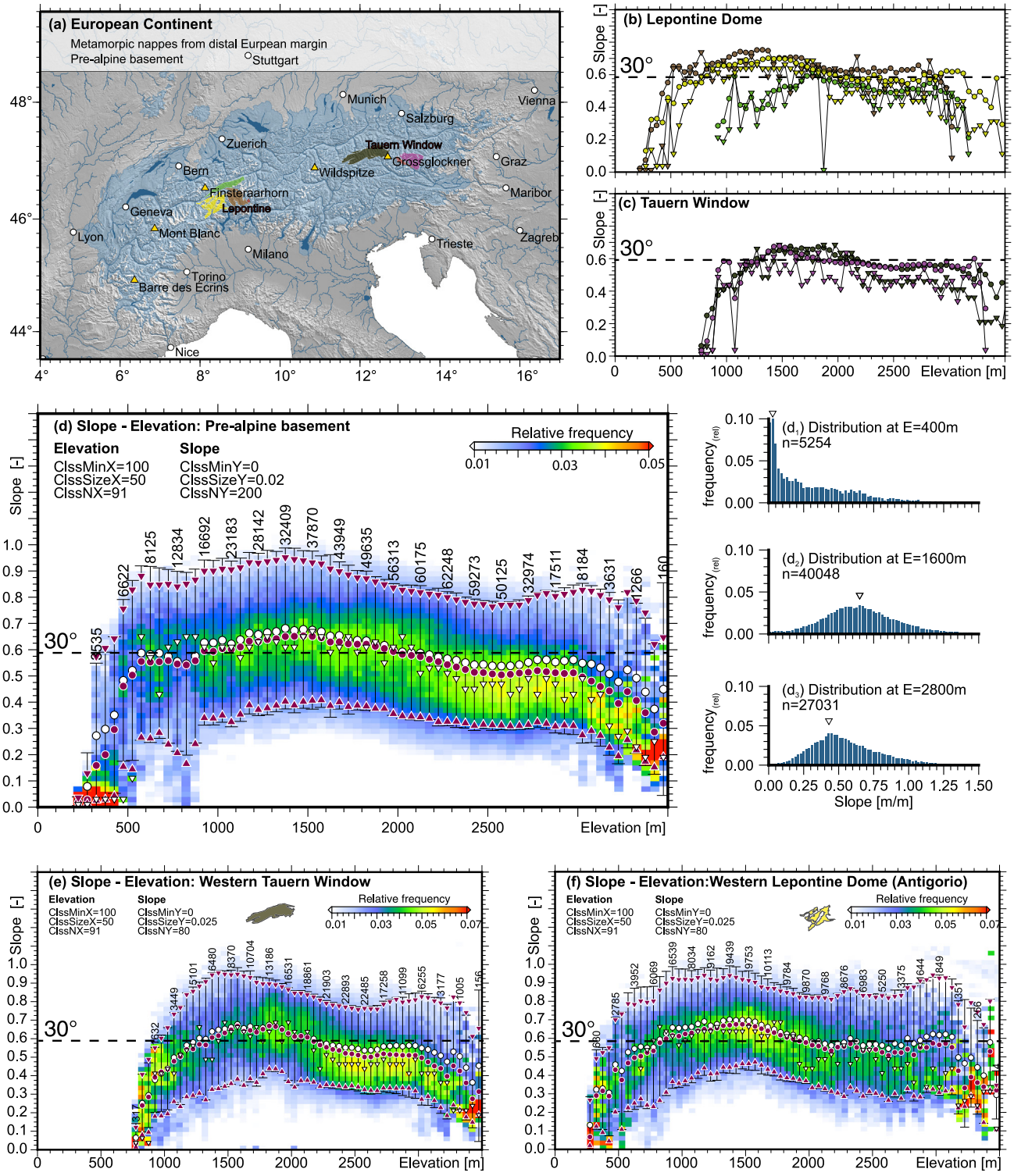

Fig. 5. Topographic pattern of the Pre-alpine basement. (a) Topographic map of the Alps and surrounding regions. Contiguous domains of the Pre-alpine basement are indicated by colored polygons. Mean (circles) and mode values (triangles) of slope at 50 m elevation slices for (b) three areas of the Lepontine and (c) two areas of the Tauern Window. Symbol colors coincide with the colors of the polygons in (a). (d) Slope–elevation distribution of all landscape patches of the Pre-alpine basement. Histograms (d_1)–(d_3) show the frequency of slopes for the entire areas of the Pre-alpine basement at E = 400 m, E = 1600 m, and E = 2800 m, respectively. (e) and (f) show the slope–elevation distributions of the Western Tauern Window and the Western Lepontine, respectively. The extent of the two domains is indicated by color-coded polygons in (a).

distribution is observed in the unglaciated Tanneron Massif at the Mediterranean coast (Fig. 6c–j).

4.1.3. Topographic similarities across the European Alps

The examples above demonstrate that the topographic expression of the European Alps with similar lithology and glacial imprint show comparable patterns in their slope–elevation relation. The transition in the slope–elevation distribution from increasing to decreasing slopes occurs between 1500 and 2000 m in all glaciated domains of the Pre-alpine basement units and External Massifs. The altitude of the local maximum coincides conspicuously well with the reported elevation range of the LGM ELA for the European Alps (e.g. Ivy-Ochs et al., 2008)

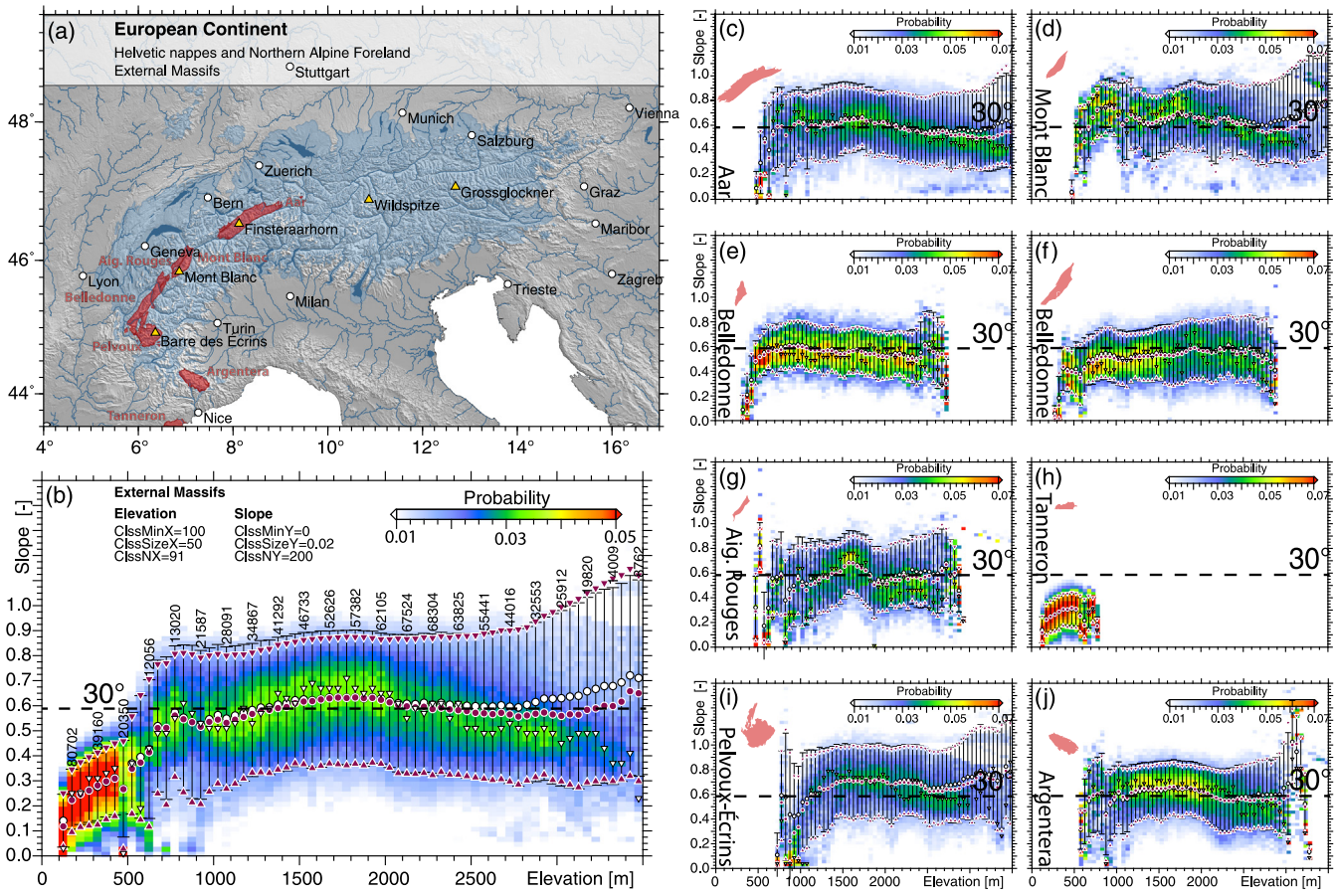

Fig. 6. Topographic pattern of the External Massifs. (a) Topographic map of the Alps and surrounding regions. Contiguous domains of the External Massifs are annotated and indicated by red polygons. (b) Slope–elevation distribution of all landscape patches of the External Massifs. (c)–(j) show the slope–elevation distribution of contiguous domains represented by polygons in (a). (For interpretation of the references to color in this figure legend, the reader is referred to the web version of this article.)

and is therefore consistent with the glacial buzz-saw hypothesis. However, the southernmost External Massif, the Argentera Massif, is located outside the contiguously glaciated part of the Alps but also shows a topographic expression characteristic for glaciated domains with its most prominent features: a local maximum of slope in an elevation range consistent with the LGM ELA, and a generally high standard deviation (Figs. 1c, 3, 6j). This nourishes the suspicion that the amount of glaciation was underestimated for the southern massifs (e.g. Ehlers et al., 2011).

4.2. Lithological effects

The lithology dependence of topographic signatures observed in slope–elevation distributions (Figs. 4, 5) is further tested by comparing eleven homogenous and adjacent structural units of the Central Alps. The chosen domains were covered by an ice cap during the LGM and precursor glaciations and align to a north–south transect from the Subalpine Molasse to the Adamello intrusion (Figs. 3, 7). A comparison of the individual slope–elevation distributions shows considerable variations among adjacent domains and confirms that the lithological inventory represents as a first-order parameter for alpine landscape evolution. Despite all differences, the structural units can be grouped according to clearly distinguishable patterns in their topographic expressions.

The most obvious pattern is found in structural units consisting of high grade metamorphic rocks like the Silvretta nappe system and magmatic intrusions as the Adamello pluton (Fig. 7h, j, k, l). This pattern is consistent with the slope–elevation distributions of the Tauern Window and the Lepontine (Fig. 5) and the External Massifs (Fig. 6) as well as with the hypothetical signal of glacially coined mountain landscapes (Fig. 1c). In addition, the transition from increasing to decreasing slopes with surface elevation is located roughly at 1700 m which is well in line with the proposed LGM ELA (e.g. Ivy-Ochs et al., 2008).

The Engadin Window and the Sesvenna domain consisting of Permo-Mesozoic rocks (Fig. 7f, i) are located adjacent to the domains described above but are characterized by a contrasting slope–elevation distribution. Here, slopes continuously steepen with elevation as described in detail for the Stammerspitze located within the Engadin Window (Fig. 4b). Despite a glacial history similar to adjacent domains, the alpine topography does not conform to the conceptual glacial slope–elevation distribution (Fig. 1c) and also lacks the local slope maximum at about 1700 m reported above. Consequently, the persistence of non-equilibrium landforms in rocks related to the Valais Ocean (e.g. Bündner Schiefer) is lower than in the gneisses of the Ötztal Crystalline or the granitic rocks of the Adamello.

The Bavarian and the Tyrolean nappes of the NCA and their tectonostratigraphic base, the Greywacke zone, show uniform slope–elevation distributions, but do not conform to any of the concepts in Fig. 1 at first glance. However, the local slope maximum of all three slope–elevation patterns is located between 1500 and 1800 m (Fig. 7d, e, g). In addition, pronounced depressions in the slope–elevation distributions of the Bavarian nappes and the Noric nappes of the Greywacke zone located at 2100 and 1700 m, respectively, correlate well in altitude with the abundant occurrence of glacial cirques in these domains. A major difference between these domains is the standard deviation of slopes in all elevation slices which is much lower for the Greywacke

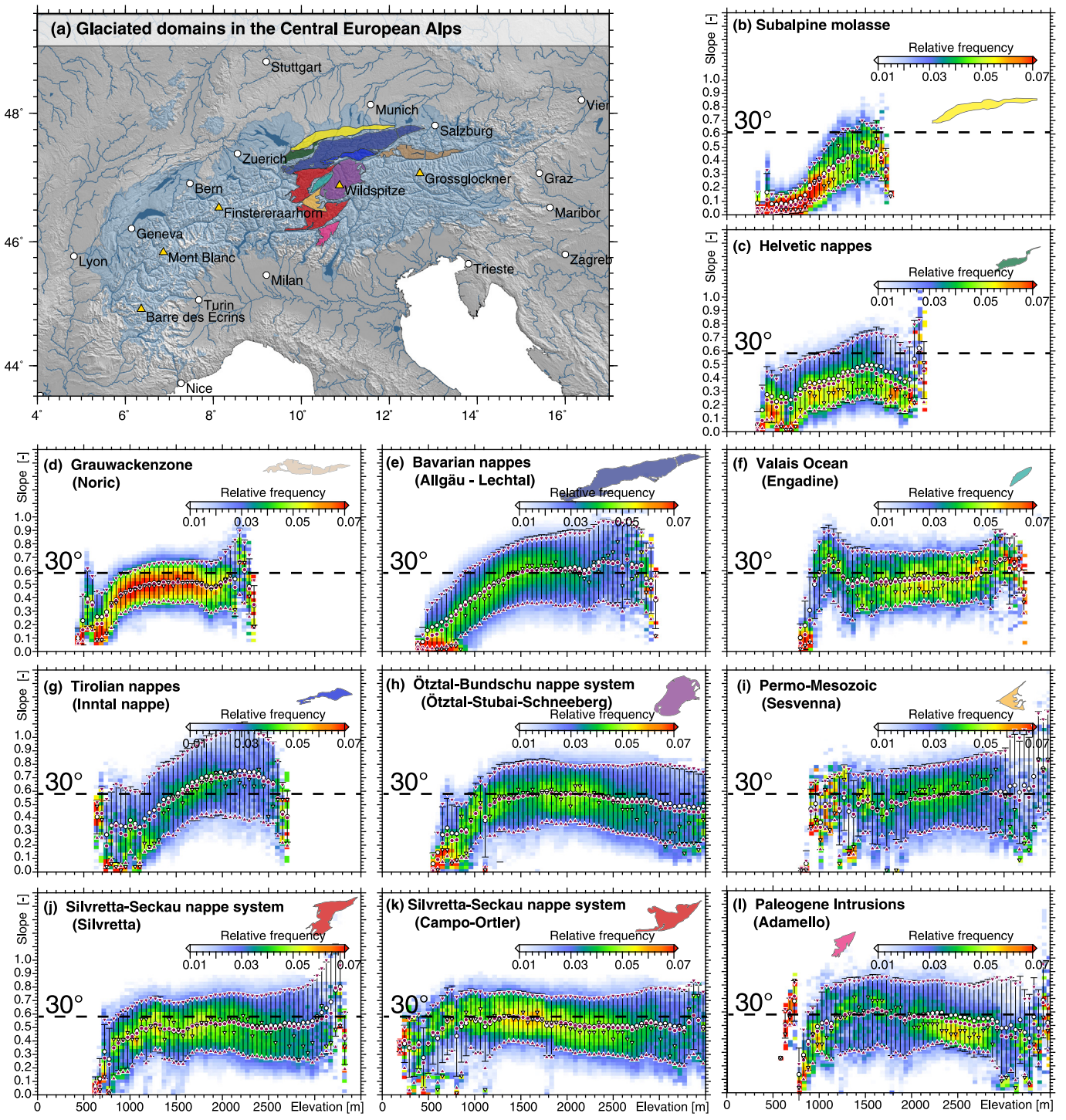

Fig. 7. Topographic pattern of 11 adjacent contiguous domains of contrasting structural units in the glaciated part of the Central Alps. (a) Topographic map of the European Alps and surrounding regions. Contiguous domains of different structural units are indicated by color-coded polygons. (b)–(l) show the slope–elevation distribution of contiguous domains represented by polygons in (a).

zone indicating rocks less resistant to erosion and the rapid decay of small scale steep glacial landforms. This goes along with reduced topographic gradients over all elevation slices which were already observed by Szekely (2001) and Szekely et al. (2002).

At the northern border of the Alps, numerous lakes and gargantuan moraines indicate a strong glacial imprint due to Piedmont glaciers which should be represented somehow in the slope–elevation distribution of the Subalpine Molasse (Fig. 7b). The highest portions of this region barely reach the LGM ELA, and therefore glacial cirques did not evolve, hence the slope–elevation distribution only represents the sub-ELA segment of the conceptual glacial signal (Fig. 1c). The turn in slope widely missing in the Subalpine Molasse is clearly detected roughly at 1600 m in the about 400 m higher mountains of the Helvetic nappes (Fig. 7c). In both domains a bimodal landscape comprising of flat valley floors and steep flanks is detected in the scatter of the mode values. As common for glaciated regions, a large standard deviation of the slope values exists throughout the entire slope–elevation distribution.

The observed topographic patterns of all eleven domains are well in line with the glacial buzz-saw concept, but the persistence of glacial morphology varies significantly with lithology.

4.3. Tectonic effects

The predominant part of the European Alps experienced significant glacial impact during the Pleistocene, while the transition zone from the Eastern Alps to the Pannonian Basin and the southern termination of the Western Alps were never or only slightly glaciated (Figs. 3, 8). This facilitates exploring the state of equilibrium of these parts of the European Alps without the disturbance by glacial erosion.

The analysis of eight homogeneous domains of the Eastern Alps (Fig. 8b–i) and six domains of the Western Alps (Fig. 8j–o) reveals a strong lithology-dependence of the topographic expressions. In addition, a transition from increasing to decreasing slopes with elevation is detected similar to glaciated regions, which conforms to the concepts outlined in Fig. 1. In contrast to glacially coined areas, the turning point in the slope–elevation distributions is located at different vertical positions in the Western and Eastern Alps. Within both regions and in strong contrast to areas within the LGM extent the standard deviation for slopes is significantly lower.

4.3.1. Non-glaciated domains of the Eastern Alps

In the non-glaciated domains of the Eastern Alps topographic gradients are lower over the entire elevation range compared to the glaciated structural units described above and the local maxima in the slope–elevation distributions are located between 800 and 1200 m hence far below the LGM ELA. Some areas like the Semmering Wechsel (Fig. 8b), the Strallegg (Fig. 8f), and the Pohorje (Figs. 8g, 4d) are characterized by spacious, gentle surfaces at high altitudes and incised channels with steep hillslopes at lower elevations. The Paleozoic of Graz shows a similar pattern except for a small area at the highest elevation range above 1500 m where numerous vertical faces consisting of karstifiable limestone lead to the gentle summit region (Fig. 8c). The slope–elevation distributions for these regions are well in line with the proposed hypothetical slope–elevation relation for a premature landscape in a fluvially dominated environment (Fig. 1a). Similar but less distinct patterns are also observed in the slope–elevation distributions of the Koralpe, Saualpe, and Gleinalpe, with the first two mountain ranges showing extremely low topographic gradients (Fig. 8d, e, h). The increased standard deviation between 500 and 1000 m due to the occurrence of a considerable amount of slopes at and above 30° coincides well with deeply incised torrents and corresponding steep hillslopes. All three mountain ranges feature a maximum in slope at the summit regions roughly at 2000 m which corresponds nicely to the occurrence of small scale, isolated cirques. Beside of small scale glacial disturbances near the peaks, the slope–elevation distribution of the Gleinalpe with small standard deviations in slope and a local maximum in the slope–elevation distribution at roughly 1200 m conforms to prematurity. The Bavarian nappes of the “Ybbstaler Alpen” consist of carbonatic rocks with a significant amount of subsurface run-off. They are characterized by a bimodal landscape with steep faces and plateaus featuring a long term persistence of landforms due to karstification indicating the high diversity of topographic expressions due to lithology-dependence (Fig. 8i).

4.3.2. Non-glaciated domains of the Western Alps

The homogeneous structural units of the non-glaciated Western Alps are several hundred kilometers apart from the eastern border of the European Alps and show striking geomorphic features as well. The deformed Mesozoic cover of the “Dauphiné-Provence” region features a slope–elevation distribution with a continuous increase of slope with altitude interpretable as a geomorphic steady-state for uplift rates increasing nonlinearly from the peripheral lowlands to the mountains (Fig. 8m). The Mono-metamorphic cover near Castelmagno and Stroppo (Briançonnais) and the Bündner Schiefer (South Penninic ophiolites) of the Voltri region display a similar bow-shaped slope–elevation pattern as the Pohorje in the Eastern Alps, even though the transition from increasing to decreasing slopes with elevation in the first of the two areas is roughly located at 1500 m and the mean slope is significantly higher over the entire elevation range (Fig. 8g, j, k). However, there are no signs of a glacial history present in these structural units but their topographic expression is consistent with a premature state of the landscape. The Zone Houlliere in the Ligurian Alps and the Variscian basement nappes of the Dora Maira are located outside the contiguously glaciated Alps (Ehlers et al., 2011) and the lower three quarters of the slope–elevation distributions are similar to the units described previously. In contrast, standard deviations increase considerably in the upper quarter. This is complemented by a bimodal landscape caused by the coexistence of steep and flat terrain conforming to glacial landforms limited to summit regions. The Argentera Massif shows the same features in the topographic expression as all External Massifs in the glaciated part of the Alps. This includes a generally high standard deviation and a local maximum in slope located between 1500 and 2000 m suggesting extensive glacial sculpting contradicting the dataset of Ehlers et al. (2011) in this region.

The non-glaciated domains of the Alps show a transition from increasing to decreasing slopes consistent with the conceptual signal of a premature fluvial landscape (Fig. 1a). These domains feature local maxima in the slope–elevation distributions at various altitudes frequently located below the LGM ELA. They are characterized by a lower standard deviation in slope compared to domains located within the LGM extent. Glacial imprint limited to high altitudes exists in several structural units at the periphery of the Western and also Eastern Alps and is clearly detectable via a strong increase in the standard deviation of slope. However, the presence of these small glacial perturbations does not contradict the conception of a pre-Pleistocene non-equilibrium landscape.

5. Discussion

The slope–elevation distributions from contiguous domains of the main structural units of the Alps show a peculiar bow-shaped pattern with a turning point in slope in glaciated and unglaciated domains throughout the orogen. The absence of this pattern in some areas is distinctly related with lithology and higher process rates towards steady-state hillslopes. To separate the glacial from the tectonic effects on the topography of the Alps we (5.1) confront differences in the slope–elevation distributions from glaciated and unglaciated areas, (5.2) explore the time-dependent evolution of slope–elevation distributions with a 2-dimensional numerical model and (5.3) present a consistent interpretation for the apparently contradicting observation of a local maximum in slope at intermediate altitudes in both realms: the glaciated and the never glaciated.

5.1. Slope–elevation relationship for glaciated versus unglaciated areas

In the glaciated realm, the surface expression originated from glacial erosion during the Pleistocene climate depression and is manifested in the slope–elevation distribution. The transition from increasing to decreasing slopes occurs roughly at similar altitudes throughout the glaciated orogen and conforms to the vertical position of the LGM ELA. This suggests a glacial origin for this morpho-metric predicted by the glacial buzz-saw hypothesis. In contrast, a tectonic cause would imply alpine-wide uniform uplift rates and synchronous onset contradicting recent geodetic leveling data within the Alps (Ruess and Höggerl, 2002; Schlatter et al., 2005) as well as the reported uplift and erosion patterns recorded in the Molasse Basin since 8 Ma (Genser et al., 2007; Cederbom et al., 2011; Gusterhuber et al., 2012). The standard deviations of slope in glaciated areas clearly exceed those of the non-glaciated regions with a strong increase above the LGM ELA. This is caused by low-

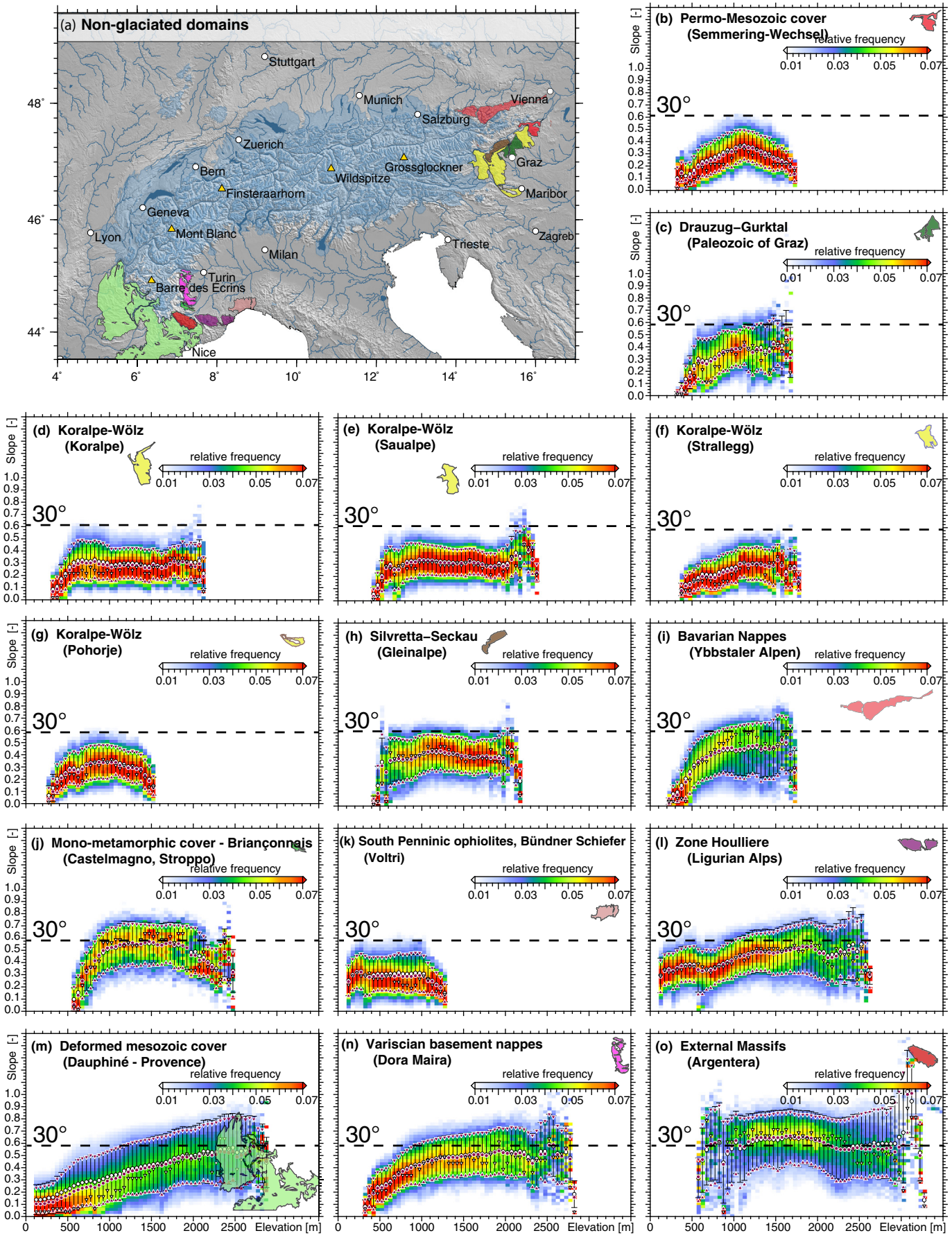
(a) Non-glaciated domains
Stuttgart
Munich
Vienna
Salzburg
Zuerich
Grossglockner
Graz
Bern
Wildspitze
Finsteraarhorn
Maribor
Geneva
Lyon
Mont Blanc
Zagreb
Trieste
Milan
Turin
Barre des Ecrins
Nice
48°
46°
44°
4°
6°
8°
10°
12°
14°
16°
(b) Permo-Mesozoic cover (Semmering-Wechsel)
(c) Drauzug–Gurktal (Paleozoic of Graz)
(d) Koralpe-Wölz (Koralpe)
(e) Koralpe-Wölz (Saualpe)
(f) Koralpe-Wölz (Strallegg)
(g) Koralpe-Wölz (Pohorje)
(h) Silvretta–Seckau (Gleinalpe)
(i) Bavarian Nappes (Ybbstaler Alpen)
(j) Mono-metamorphic cover - Briançonnais (Castelmagno, Stroppo)
(k) South Penninic ophiolites, Bündner Schiefer (Voltri)
(l) Zone Houlliere (Ligurian Alps)
(m) Deformed mesozoic cover (Dauphiné - Provence)
(n) Variscian basement nappes (Dora Maira)
(o) External Massifs (Argentera)
relative frequency
0.01 0.03 0.05 0.07
30°
Slope [-]
Elevation [m]
0 500 1000 1500 2000 2500

gradient cirque floors occurring in concert with steep cirque walls, ridges, and horns. However, the existence and persistence of the glacial topographic expression vary with lithological properties. This is clearly documented by the landforms of adjacent domains with contrasting lithological inventory. While glaciated landscapes are preserved in rocks of low erodibility (e.g. granitic rocks of the Adamello) glacial characteristics can hardly be detected in highly erodible rocks (e.g. schists of the Engadin). Following the slope stability concept this may be best explained by higher surface process rates in over-steepened terrain and therefore an advanced state of glacial-to-fluvial landscape transition.

In the non-glaciated realm, the topographic expression depends on lithology as well, indicated by variations in mean and maximum slopes. In comparable structural units, the standard deviation in slope is significantly lower in domains outside the LGM extent compared with the glaciated counterparts. Spectacularly, never glaciated regions also feature a transition from increasing to decreasing slopes. In contrast to glaciated areas, these local maxima are located at various altitudes and generally far below the LGM ELA at the eastern border of the Alps. This suggests a tectonically rather than a glacially influenced surface expression representing a premature landscape. The slope–elevation distribution of such a tectonically controlled non-equilibrium is most prominently observed at the transition from the Eastern Alps to the Pannonian Basin but there is also evidence for a similar signal in the Western Alps. Consequently, the question arises whether the prematurity observed at the fringe of the Alps can be representative for the entire mountain range as proposed by Hergarten et al. (2010) and is superimposed by a glacial signal leading to the observation of glacially-sculpted and tectonically-driven landscapes. Small glacial perturbations in domains outside the contiguous LGM extent (e.g. Fig. 8e) gives a clue on how a premature topography is partly transformed to feature glacial landscape characteristics. An extensive transformation towards a fully featured glacial landscape can be expected within the LGM extent.

5.2. From prematurity towards a steady-state slope–elevation distribution

In order to interpret the bow shaped slope–elevation distribution from the non-glaciated parts of the Alps with a transition from increasing to decreasing topographic gradients at various altitudes we revisit the numerical study of Robl et al. (2008b) and explore the development of topography and related statistical metrics over time. For this, we apply a 2-dimensional numerical model describing the collision of the Adriatic indenter with Europe by a thin viscous sheet approach (England and McKenzie, 1982; Houseman and England, 1986; Robl and Stüwe, 2005) coupled with a detachment limited, stream power-based landscape evolution model (Howard, 1994; Hergarten, 2002). Boundary conditions describing convergence and east-directed lateral extrusion, geometry of domains featuring contrasting rheology, position of four pre-defined faults and model parameters for viscous deformation and fluvial erosion are explained in detail by Robl et al. (2008b).

In addition to tectonic constraints on extension in the Eastern Alps during continental convergence the model results are also consistent with many first-order topographic features including the drainage system, the position of the main drainage divides, the occurrence of orogen-parallel valleys and characteristic elbow shaped bends of the main streams. The topographic evolution and state of maturity of the virtual Eastern Alps are explored at different time slices where rising topography and increasing topographic gradients towards steady-state are directly observed (Fig. 9).

After 10 Ma of convergence a complex topographic pattern develops due to contrasts in rheology, the geometry of the Adriatic indenter, faults, and the applied boundary conditions describing the counterclockwise rotation of the Adriatic plate with a maximum convergence rate of 10 mm/y at the easternmost edge of the indenter and zero stress eastern boundary allowing lateral extrusion towards the Pannonian basin. The evolution of drainage systems is controlled by gradients of the rising topography. Fluvial equilibrium is induced from the low lying forelands towards the elevated but gently sloped center of the orogen. This is indicated by the fluvial pattern of erosion that develops over time by the upstream migration of knick points separating non-equilibrium paleo-surfaces from landscape patches where uplift rates are already balanced by erosion rates. This leads to the development of a typical bow-shaped slope–elevation distribution which is well in line with the signal of a non-equilibrium fluvial landscape (Fig. 1a) and frequently observed within the never glaciated fringe of the Eastern Alps.

After 20 Ma of convergence large areas of the orogen are still in a transient state represented by the pronounced transition from increasing to decreasing slopes with surface elevation and plateaus at high altitudes. Near steady-state is reached at about 30 Ma of convergence. Nevertheless, even at this time step, the fraction of surface patches in a transient state increases with altitude represented by decreasing slopes. Topographic gradients of the model topography are in general lower than in the European Alps and are controlled by the contributing drainage area according to the detachment limited stream power approach describing fluvial erosion. Due to the spatial resolution of the mesh, small contributing drainage areas and therefore steep slopes are missing in the model results. Timing and rates towards morphological equilibrium depend on the erodibility of rocks, a property that is still not well constrained.

However, the observed relation of slope and elevation in of the European Alps can largely be reproduced by a numerical model that accounts for crustal shortening, tectonically driven uplift and fluvial erosion without considering glacial effects. This clearly indicates that a transition from increasing to decreasing slopes in orogens is not necessarily a result of glacial imprint but may be caused by crustal thickening as a consequence of plate convergence or by other tectonic causes leading to accelerated uplift (e.g. slab break-off). In a fluvial non-equilibrium landscape, the vertical position of the turning point in the slope–elevation distribution is a measure of maturity and may be located at different elevations for spatiotemporal variations in uplift rate and rock erodibility. This explains that the transition from increasing to decreasing slopes with elevation becomes more gradual over time in a complex collisional orogen like the European Alps and demands for an analysis spatially constrained to individual structural units as performed in this study.

5.3. Recent uplift and a climate depression

As clearly shown by the results of the numerical description of the Eastern Alps, fluvial prematurity is characterized by a bow-shaped slope–elevation distribution with a distinct local maximum in slope at intermediate elevations. The position of the turning point migrates to higher elevations with increasing maturity of the range and may therefore be interpreted as rough metric for the state of equilibrium of the orogen, so that recent uplift can be detected by our analysis.

A recent pulse of tectonic uplift has affected at least the Eastern Alps and is manifested by the sedimentary record of the adjacent Northern Molasse basin (Genser et al., 2007; Cederbom et al., 2011; Gusterhuber et al., 2012), the occurrence of strath terraces along major alpine rivers at the transition from the Eastern Alps to the Pannonian Basin (Wagner et al., 2011), and burial ages from fluvial

Fig. 8. Topographic pattern of 14 adjacent contiguous domains of contrasting structural units in the non-glaciated periphery of the European Alps. (a) Topographic map of the European Alps and surrounding regions. Contiguous domains of different structural units indicated by color-coded polygons. (b)–(o) show the slope–elevation distribution of contiguous domains represented by polygons in (a).

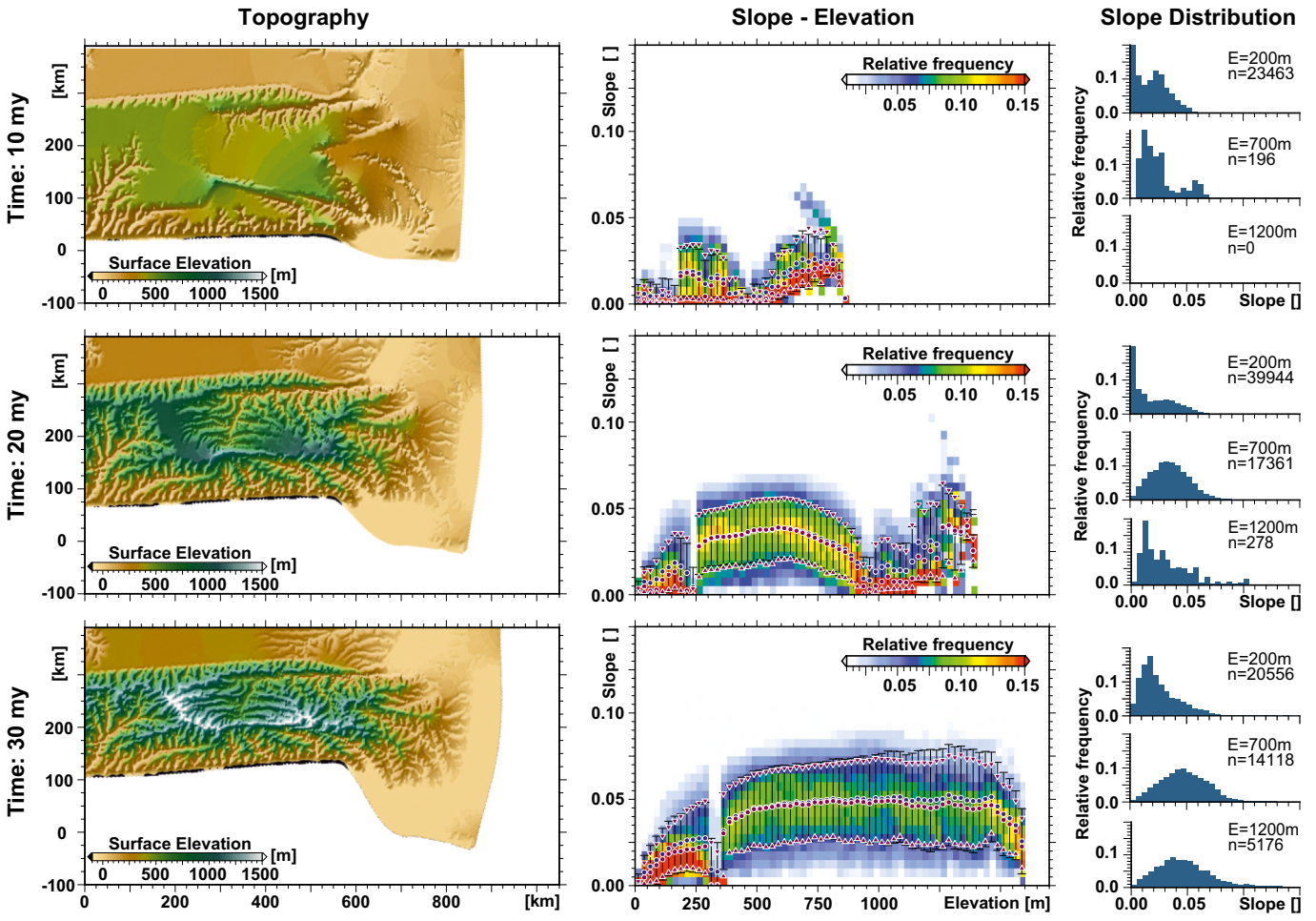

Fig. 9. Time-dependent evolution of alpine topography based on a coupled numerical model (Robl et al., 2008b) for three different time steps and the corresponding slope–elevation distributions. Lines and symbols in the figure correspond to Fig. 2. Note that the obvious planation surface at north of the orogenic wedge represents a hard block in the mechanical module of the model (passive indenter of the northern foreland) and causes the low gradient elevation slice in the slope–elevation distributions roughly at 250 m.

pebbles in caves (Wagner et al., 2010; Meyer et al., 2011). In addition, very low exhumation and long-term erosion rates in the central uplands of the Eastern Alps (e.g. Ötztal Crystalline — northwest of the tip of the Adriatic indenter; (Baran et al., 2014)) and an increase of the sediment delivery from the Alps to the foreland basins over the last 5 Ma (e.g. Kuhlemann, 2007) imply low topographic gradients present at high altitudes before the onset of alpine glaciations. This is consistent with a pre-Pleistocene non-equilibrium landscape caused by increased uplift rates in the recent geological past. A similar topographic pattern develops in numerical experiments for the Eastern Alps. After about 20 Ma of convergence and most prominent northwest of the indenter tip the model shows low gradient paleo-surfaces in higher altitudes that are characterized by lower erosion rates and less exhumation compared to the surrounding already equilibrated low-lying areas (Fig. 9).

Whatever process causes or contributes to the present uplift pattern, a pre-Pleistocene pulse of uplift accompanied by prematurity of the European Alps would have essentially influenced onset and extent of the Pleistocene alpine glaciations. Uplift of the non-equilibrium alpine topography and synchronous global cooling during Plio–Pleistocene times (e.g. Zachos et al., 2001) would position spacious low-gradient areas at or above the ELA. These large elevated paleo-surfaces represented by areal maxima in the hypsometric curve would promote the accumulation of ice in a similar way as suggested by Pedersen and Egholm (2013) for glacially preconditioned terrain during repeated glaciation cycles. This may happen due to surface uplift, climate depression, or both. Once the areal maxima are covered by glaciers, glacial erosion would adjust the vertical position of these maxima to the ELA. This would be indicated by a similar vertical position of the turning point in slope throughout the glaciated part of the Alps conforming to both the glacial buzz-saw hypothesis and the prematurity of the alpine orogen. Consequently, another facet can be added to the chicken and egg problem of topography development in the European Alps: a major part of the most recent uplift rates may be accredited to erosional unloading and isostatic rebound (Kuhlemann et al., 2002; Champagnac et al., 2007), but onset and extent of Pleistocene glaciation may have been heavily influenced by surface uplift driven by tectonics.

6. Conclusion

The main results of our analysis of the relationship between slope and surface elevation for contiguous domains of important structural units of the European Alps are:

a. Large parts of the European Alps are characterized by a transition from increasing to decreasing slopes at intermediate altitudes between 1500 and 2000 m. This pattern is consistent with both a transient landscape that may be explained by fluvial prematurity due to recent uplift (Hergarten et al., 2010) and with the concept of the glacial buzz-saw (e.g. Brozović et al., 1997) as well.
b. A detailed analysis of slope–elevation distributions for contiguous domains of the main structural units of the Alps clearly indicates a strong lithology-dependence of the topographic expression. We interpret contrasting slope–elevation patterns of adjacent domains with a similar glacial and tectonic history as a result of the highly

variable process celerity towards steady-state slopes for different lithological inventories.

c. All over the glaciated realm of the Alps high-grade metamorphic (e.g. External Massifs) or magmatic rocks (e.g. Adamello intrusion) are characterized by a transition from increasing to decreasing slopes roughly at the LGM ELA, while this signal has vanished in rocks related to the Valais ocean (e.g. Engadin Window). We interpret the local maximum in slope at the LGM ELA as the impact of the glacial buzz-saw and the long term persistence of glacial landforms. These domains may also feature inherited glacial landforms from precursor glaciations.
d. A transition from increasing to decreasing slopes with elevation is also explored beyond the LGM extent, but the vertical position of the turning point varies and is in generally located below the LGM ELA. We interpret this pattern as evidence for young tectonically driven uplift. This uplift event may have affected large parts of the European Alps but was overprinted by the Pleistocene glaciation cycles.
e. Our interpretation is supported by numerical modeling results that reproduce the observed slope–elevation distribution of the European Alps by numerically describing crustal shortening, tectonically driven uplift and fluvial erosion, but neglecting glacial effects.
f. Our interpretation is also consistent with proposed uplift rates from the non-glaciated eastern border of the Alps (Frisch et al., 2000; Wagner et al., 2010; Wagner et al., 2011) and from adjacent basins (Genser et al., 2007; Cederbom et al., 2011; Gusterhuber et al., 2012), and allows to expand these findings also to the glaciated parts of the Alps.
g. We suggest that a large scale recent pulse of surface uplift driven by tectonics may have heavily influenced onset and extent of the glaciation during the Pleistocene climate depression. The tectonic signal of this recent pulse of uplift – a local maximum in slope at various vertical positions – is superimposed by the signal of the glacial buzz-saw so that the turning point in the slope-elevation distributions within the LGM extent becomes located roughly at the LGM ELA. Fluvial prematurity is therefore only directly observed at the fringe of the orogen but it is likely that large parts of the orogen were in a premature state with a transition from increasing to decreasing slopes at intermediate altitudes even before the onset of the Pleistocene glaciation cycles.

Acknowledgment

This work was financially supported by the Austrian Science Fund (FWF) through the Doctoral College GIScience [W1237-N23]. Ruedi Homberger is thanked for providing four gorgeous aerial photos of the European Alps. We thank two anonymous reviewers for many suggestions that have greatly improved this manuscript.

References

Baran, R., Friedrich, A.M., Schlunegger, F., 2014. The late Miocene to Holocene erosion pattern of the Alpine foreland basin reflects Eurasian slab unloading beneath the western Alps rather than global climate change. Lithosphere 6 (2), 124–131.
Bousquet, R., Schmid, S.M., Zeilinger, G., Oberhänsli, R., Rosenberg, C.L., Molli, G., Wiederkehr, M., Rossi, P., 2012. Tectonic Framework of the Alps. CCGM/CGMQ, Paris, France.
Brozović, N., Burbank, D.W., Meigs, A.J., 1997. Climatic limits on landscape development in the northwestern Himalaya. Science 276 (5312), 571–574.
Cederbom, C.E., van der Beek, P., Schlunegger, F., Sinclair, H.D., Oncken, O., 2011. Rapid extensive erosion of the North Alpine foreland basin at 5–4 Ma. Basin Res. 23 (5), 528–550.
Champagnac, J.D., Molnar, P., Anderson, R.S., Sue, C., Delacou, B., 2007. Quaternary erosion-induced isostatic rebound in the western Alps. Geology 35 (3), 195.
Champagnac, J.-D., Schlunegger, F., Norton, K., von Blanckenburg, F., Abbühl, L.M., Schwab, M., 2009. Erosion-driven uplift of the modern Central Alps. Tectonophysics 474 (1–2), 236–249.
Duretz, T., Gerya, T.V., May, D.A., 2011. Numerical modelling of spontaneous slab breakoff and subsequent topographic response. Tectonophysics 502 (1–2), 244–256.
Egholm, D.L., Nielsen, S.B., Pedersen, V.K., Lesemann, J.E., 2009. Glacial effects limiting mountain height. Nature 460 (7257), 884–887.
Ehlers, J., Gibbard, P.L., Hughes, P.D., 2011. Quaternary glaciations-extent and chronology: a closer look, 15. Elsevier.
England, P., McKenzie, D., 1982. A thin viscous sheet model for continental deformation. Geophys. J. R. Astron. Soc. 70 (2), 295–321.
Farr, T.G., Kobrick, M., 2000. Shuttle radar topography mission produces wealth of data. Am. Geophys. Union Eos 81, 583–585.
Frisch, W., Kuhlemann, J., Dunkl, I., Brügel, A., 1998. Palinspastic reconstruction and topographic evolution of the Eastern Alps during late tertiary tectonic extrusion. Tectonophysics 297, 1–15.
Frisch, W., Szekely, B., Kuhlemann, J., Dunkl, I., 2000. Geomorphological evolution of the Eastern Alps in response to Miocene tectonics. Z. Geomorph. 44, 103–138.
Frisch, W., Kuhlemann, J., Dunkl, I., Szekely, B., 2001. The Dachstein paleosurface and the Augenstein Formation in the Northern Calcareous Alps; a mosaic stone in the geomorphological evolution of the Eastern Alps. Int. J. Earth Sci. 90, 500–518.
Garzanti, E., Vezzoli, G., Andò, S., 2011. Paleogeographic and paleodrainage changes during Pleistocene glaciations (Po Plain, Northern Italy). Earth Sci. Rev. 105 (1–2), 25–48.
Genser, J., Cloetingh, S., Neubauer, F., 2007. Late orogenic rebound and oblique Alpine convergence: new constraints from subsidence analysis of the Austrian Molasse basin. Glob. Planet. Chang. 58 (1–4), 214–223.
Gudmundsson, G.H., 1994. An order-of-magnitude estimate of the current uplift-rates in Switzerland caused by the Wurm Alpine deglaciation. Eclogae Geol. Helv. 87 (2), 545–557.
Gusterhuber, J., Dunkl, I., Hinsch, R., Linzer, H.G., Sachsenhofer, R.F., 2012. Neogene uplift and erosion in the Alpine Foreland Basin (Upper Austria and Salzburg). Geol. Carpath. 63 (4), 295–305.
Haeuselmann, P., Granger, D.E., Jeannin, P.-Y., Lauritzen, S.-E., 2007. Abrupt glacial valley incision at 0.8 Ma dated from cave deposits in Switzerland. Geology 35 (2), 143–146.
Hergarten, S., 2002. Self Organised Criticality in Earth Systems. Springer, Heidelberg (272 pp.).
Hergarten, S., Wagner, T., Stüwe, K., 2010. Age and prematurity of the Alps derived from topography. Earth Planet. Sci. Lett. 297 (3–4), 453–460.
Herman, F., Beaud, F., Champagnac, J.-D., Lemieux, J.-M., Sternai, P., 2011. Glacial hydrology and erosion patterns: a mechanism for carving glacial valleys. Earth Planet. Sci. Lett. 310 (3–4), 498–508.
Hinderer, M., Kastowski, M., Kamelger, A., Bartolini, C., Schlunegger, F., 2013. River loads and modern denudation of the Alps — a review. Earth Sci. Rev. 118, 11–44.
Houseman, G., England, P., 1986. Finite strain calculations of continental deformation: 1. Method and general results for convergent zones. J. Geophys. Res. B: Solid Earth 91 (B3), 3651–3663.
Howard, A.D., 1994. A detachment-limited model of drainage basin evolution. Water Resour. Res. 30 (7), 2261–2285.
Hurst, M.D., Mudd, S.M., Yoo, K., Attal, M., Walcott, R., 2013. Influence of lithology on hillslope morphology and response to tectonic forcing in the northern Sierra Nevada of California. J. Geophys. Res. F: Earth Surf. 118 (2), 832–851.
Ivy-Ochs, S., Kerschner, H., Reuther, A., Maisch, M., Sailer, R., Schaefer, J., Kubik, P.W., Synal, H.A., Schlüchter, C., 2006. The timing of glacier advances in the northern European Alps based on surface exposure dating with cosmogenic 10Be, 26Al, 36Cl, and 21Ne. pp. 43–60.
Ivy-Ochs, S., Kerschner, H., Reuther, A., Preusser, F., Heine, K., Maisch, M., Kubik, P.W., Schlüchter, C., 2008. Chronology of the last glacial cycle in the European Alps. J. Quat. Sci. 23 (6–7), 559–573.
Keil, M., Neubauer, F., 2011. Neotectonics, drainage pattern and geomorphology of the orogen-parallel Upper Enns Valley (Eastern Alps). Geol. Carpath. 62 (3).
Korup, O., Weidinger, J.T., 2011. Rock Type, Precipitation, and the Steepness of Himalayan Threshold Hillslopes. pp. 235–249.
Kuhlemann, J., 2007. Paleogeographic and paleotopographic evolution of the Swiss and Eastern Alps since the Oligocene. Glob. Planet. Chang. 58 (1–4), 224–236.
Kuhlemann, J., Frisch, W., Szekely, B., Dunkl, I., Kázmér, M., 2002. Post-collisional sediment budget history of the Alps: tectonic versus climatic control. Int. J. Earth Sci. 91 (5), 818–837.
Kühni, A., Pfiffner, O.A., 2001. The relief of the Swiss Alps and adjacent areas and its relation to lithology and structure: topographic analysis from a 250-m DEM. Geomorphology 41 (4), 285–307.
Legrain, N., Stüwe, K., Wölfler, A., 2014a. Incised relict landscapes in the eastern Alps. Geomorphology 221, 124–138.
Legrain, N., Dixon, J., Stüwe, K., von Blanckenburg, F., Kubik, P., 2014b. Post-Miocene landscape rejuvenation at the eastern end of the Alps. Lithosphere.
Luth, S., Willingshofer, E., Sokoutis, D., Cloetingh, S., 2013. Does subduction polarity changes below the Alps? Inferences from analogue modelling. Tectonophysics 582, 140–161.
Lyon-Caen, H., Molnar, P., 1989. Constraints on the deep structure and dynamic processes beneath the Alps and adjacent regions from an analysis of gravity anomalies. Geophys. J. Int. 99 (1), 19–32.
McNamara, J.P., Ziegler, A.D., Wood, S.H., Vogler, J.B., 2006. Channel head locations with respect to geomorphologic thresholds derived from a digital elevation model: a case study in northern Thailand. For. Ecol. Manag. 224 (1–2), 147–156.
Meyer, M.C., Cliff, R.A., Spotl, C., 2011. Speleothems and mountain uplift. Geology 39 (5), 447–450.
Monegato, G., Vezzoli, G., 2011. Post-Messinian drainage changes triggered by tectonic and climatic events (eastern Southern Alps, Italy). Sediment. Geol. 239 (3–4), 188–198.

Montgomery, D.R., 2001. Slope distributions, threshold hillslopes, and steady-state topography. Am. J. Sci. 301 (4–5), 432–454.
Montgomery, D.R., Korup, O., 2011. Preservation of inner gorges through repeated Alpine glaciations. Nat. Geosci. 4 (1), 62–67.
Muttoni, G., Carcano, C., Garzanti, E., Ghielmi, M., Piccin, A., Pini, R., Rogledi, S., Sciunnach, D., 2003. Onset of major Pleistocene glaciations in the Alps. Geology 31 (11), 989–992.
Neteler, M., Bowman, M.H., Landa, M., Metz, M., 2012. GRASS GIS: a multi-purpose open source GIS. Environ. Model Softw. 31, 124–130.
Norton, K.P., von Blanckenburg, F., Schlunegger, F., Schwab, M., Kubik, P.W., 2008. Cosmogenic nuclide-based investigation of spatial erosion and hillslope channel coupling in the transient foreland of the Swiss Alps. Geomorphology 95 (3–4), 474–486.
Norton, K.P., Abbuhl, L.M., Schlunegger, F., 2010. Glacial conditioning as an erosional driving force in the Central Alps. Geology 38 (7), 655–658.
Pedersen, V.K., Egholm, D.L., 2013. Glaciations in response to climate variations preconditioned by evolving topography. Nature 493 (7431), 206–210.
Penck, A., 1905. Glacial feature in the surface of the Alps. J. Geol. 13 (1), 1–19.
Preusser, F., Reitner, J.M., Schlüchter, C., 2010. Distribution, geometry, age and origin of overdeepened valleys and basins in the Alps and their foreland. Swiss J. Geosci. 103, 407–426.
Ratschbacher, L., Merle, O., Davy, P., Cobbold, P., 1991. Lateral extrusion in the Eastern Alps, part 1: Boundary conditions and experiments scaled for gravity. Tectonics 10 (2), 257–271.
Raumer, J.F., Ménot, R.P., Abrecht, J., Biino, G., 1993. The pre-Alpine Evolution of the External Massifs. In: Raumer, J.F., Neubauer, F. (Eds.), Pre-Mesozoic Geology in the Alps. Springer, Berlin Heidelberg, pp. 221–240.
Reitner, J.M., Gruber, W., Römer, A., Morawetz, R., 2010. Alpine overdeepenings and paleo-ice flow changes: an integrated geophysical–sedimentological case study from Tyrol (Austria). Swiss J. Geosci. 103, 385–405.
Robl, J., Stüwe, K., 2005. Continental collision with finite indenter strength: 2. European Eastern Alps. Tectonics 24 (4) (n/a-n/a).
Robl, J., Hergarten, S., Stüwe, K., 2008a. Morphological analysis of the drainage system in the Eastern Alps. Tectonophysics 460 (1–4), 263–277.
Robl, J., Stüwe, K., Hergarten, S., Evans, L., 2008b. Extension during continental convergence in the Eastern Alps: the influence of orogen-scale strike-slip faults. Geology 36, 603–606.
Ruess, D., Höggerl, N., 2002. Bestimmung rezenter Höhen- und Schwereänderungen in Österreich. In: Friedl, G., Genser, J., Handler, R., Neubauer, F., Steyrer, H.-P. (Eds.), PANGEO AUSTRIA. Universität Salzburg, Salzburg, Institut für Geologie und Paläontologie, p. 151-151.
Salcher, B.C., Kober, F., Kissling, E., Willett, S.D., 2014. Glacial impact on short-wavelength topography and long-lasting effects on the denudation of a deglaciated mountain range. Glob. Planet. Chang. 115, 59–70.
Scardia, G., De Franco, R., Muttoni, G., Rogledi, S., Caielli, G., Carcano, C., Sciunnach, D., Piccin, A., 2012. Stratigraphic evidence of a Middle Pleistocene climate-driven flexural uplift in the Alps. Tectonics 31 (6) (n/a-n/a).
Schlatter, A., Schneider, D., Geiger, A., Kahle, H.G., 2005. Recent vertical movements from precise levelling in the vicinity of the city of Basel, Switzerland. Int. J. Earth Sci. 94 (4), 507–514.
Schlunegger, F., 2002. Impact of hillslope-derived sediment supply on drainage basin development in small watersheds at the northern border of the central Alps of Switzerland. Geomorphology 46 (3–4), 285–305.
Schlunegger, F., Schneider, H., 2005. Relief-rejuvenation and topographic length scales in a fluvial drainage basin, Napf area, Central Switzerland. Geomorphology 69 (1–4), 102–117.
Schlunegger, F., Badoux, A., McArdell, B.W., Gwerder, C., Schnydrig, D., Rieke-Zapp, D., Molnar, P., 2009. Limits of sediment transfer in an alpine debris-flow catchment, Illgraben, Switzerland. Quat. Sci. Rev. 28 (11–12), 1097–1105.
Schmidt, K.M., Montgomery, D.R., 1995. Limits to relief. Science 270 (5236), 617–620.
Spotila, J.A., Buscher, J.T., Meigs, A.J., Reiners, P.W., 2004. Long-term glacial erosion of active mountain belts: example of the Chugach–St. Elias Range, Alaska. Geology 32 (6), 501–504.
Sternai, P., Herman, F., Champagnac, J.D., Fox, M., Salcher, B., Willett, S.D., 2012. Pre-glacial topography of the European Alps. Geology 40 (12), 1067–1070.
Strahler, A.N., 1950. Equilibrium theory of erosional slopes approached by frequency distribution analysis. Am. J. Sci. 248 (673–696), 800–814.
Stüwe, K., Homberger, R., 2012. High Above the Alps: A Bird's Eye View of Geology. Weishaupt Publishing, Gnas (296 pp.).
Stüwe, K., Robl, J., Hergarten, S., Evans, L., 2008. Modeling the influence of horizontal advection, deformation, and late uplift on the drainage development in the India–Asia collision zone. Tectonics 27 (6) (n/a-n/a).
Szekely, B., 2001. On the surface of the Eastern Alps — a DEM study. Tübinger Geowiss. Arb. 60, 1–124.
Szekely, B., 2003. The Eastern Alps in an envelope — an estimation on the "missing volume". N. Jb. Geol. Paläont. (Abh.) 230, 257–275.
Szekely, B., Reinecker, J., Dunkl, I., Frisch, W., Kuhlemann, J., 2002. Neotectonic movements and their geomorphic response as reflected in surface parameters and stress patterns in the Eastern Alps. EGU Stephan Müller Spec. Publ. Ser. 3, 149–166.
Valera, J.L., Negredo, A.M., Jiménez-Munt, I., 2011. Deep and near-surface consequences of root removal by asymmetric continental delamination. Tectonophysics 502 (1–2), 257–265.
van der Beek, P., Bourbon, P., 2008. A quantification of the glacial imprint on relief development in the French western Alps. Geomorphology 97 (1–2), 52–72.
Vernon, A.J., van der Beek, P.A., Sinclair, H.D., Rahn, M.K., 2008. Increase in late Neogene denudation of the European Alps confirmed by analysis of a fission-track thermochronology database. Earth Planet. Sci. Lett. 270 (3–4), 316–329.
von Blankenburg, F., Davis, J.H., 1995. Slab breakoff: a model for syncollisional magmatism and tectonics in the Alps. Tectonics 14 (1), 120–131.
Wager, L.R., 1937. The Arun River drainage pattern and the rise of the Himalaya. Geogr. J. 89 (3), 239–250.
Wagner, T., Fabel, D., Fiebig, M., Häuselmann, P., Sahy, D., Xu, S., Stüwe, K., 2010. Young uplift in the non-glaciated parts of the Eastern Alps. Earth Planet. Sci. Lett. 295 (1–2), 159–169.
Wagner, T., Fritz, H., Stuwe, K., Nestroy, O., Rodnight, H., Hellstrom, J., Benischke, R., 2011. Correlations of cave levels, stream terraces and planation surfaces along the River Mur—timing of landscape evolution along the eastern margin of the Alps. Geomorphology (Amst) 134 (1–2), 62–78.
Whipple, K.X., DiBiase, R.A., Crosby, B.T., 2013. 9.28 Bedrock Rivers. In: Shroder, J.F. (Ed.), Treatise on Geomorphology. Academic Press, San Diego, pp. 550–573.
Willett, S.D., Schlunegger, F., Picotti, V., 2006. Messinian climate change and erosional destruction of the central European Alps. Geology 34 (8), 613.
Willett, S.D., McCoy, S.W., Perron, J.T., Goren, L., Chen, C.Y., 2014. Dynamic reorganization of river basins. Science 343 (6175), 1248765.
Wittmann, H., von Blanckenburg, F., Kruesmann, T., Norton, K.P., Kubik, P.W., 2007. Relation between rock uplift and denudation from cosmogenic nuclides in river sediment in the Central Alps of Switzerland. J. Geophys. Res. Earth Surf. 112 (F4), F04010.
Zachos, J., Pagani, M., Sloan, L., Thomas, E., Billups, K., 2001. Trends, rhythms, and aberrations in global climate 65 Ma to present. Science 292 (5517), 686–693.